2018

Transcriptional repression by ApiAP2 factors is central to chronic toxoplasmosis

Joshua B. Radke
Washington University School of Medicine in St. Louis

Danielle Worth
University of California, Riverside

David Hong
University of South Florida

Sherri Huang
Indiana Univeristy School of Medicine

William J. Sullivan Jr.
Indiana University School of Medicine

See next page for additional authors

PLOS | PATHOGENS

RESEARCH ARTICLE

Transcriptional repression by ApiAP2 factors is central to chronic toxoplasmosis

Joshua B. Radke[1¤], Danielle Worth[2], David Hong[1], Sherri Huang[3], William J. Sullivan, Jr.[3], Emma H. Wilson[2], Michael W. White[1]*

1 Department of Global Health, University of South Florida, Tampa, FL, United States of America, **2** Division of Biomedical Sciences, School of Medicine, University of California, Riverside, Riverside, CA, United States of America, **3** Department of Pharmacology and Toxicology, Indiana University School of Medicine, Indianapolis, IN, United States of America

¤ Current address: Department of Molecular Microbiology, Washington University School of Medicine, St. Louis, MO, United States of America.
* mwhite.usf@gmail.com

Citation: Radke JB, Worth D, Hong D, Huang S, Sullivan WJ, Jr., Wilson EH, et al. (2018) Transcriptional repression by ApiAP2 factors is central to chronic toxoplasmosis. PLoS Pathog 14 (5): e1007035. https://doi.org/10.1371/journal.ppat.1007035

Editor: Dominique Soldati-Favre, University of Geneva, SWITZERLAND

Received: January 20, 2017

Accepted: April 17, 2018

Published: May 2, 2018

Data Availability Statement: All relevant data are within the paper and its Supporting Information files. All relevant data are also available on the BioRxiv preprint server (https://doi.org/10.1101/094847).

Funding: This study was funded by the National Institutes of Allergies and Infectious Disease (https://www.niaid.nih.gov) grant awards AI124682 and AI089885. The funders had no role in study design, data collection and analysis,

Abstract

Tachyzoite to bradyzoite development in *Toxoplasma* is marked by major changes in gene expression resulting in a parasite that expresses a new repertoire of surface antigens hidden inside a modified parasitophorous vacuole called the tissue cyst. The factors that control this important life cycle transition are not well understood. Here we describe an important transcriptional repressor mechanism controlling bradyzoite differentiation that operates in the tachyzoite stage. The ApiAP2 factor, AP2IV-4, is a nuclear factor dynamically expressed in late S phase through mitosis/cytokinesis of the tachyzoite cell cycle. Remarkably, deletion of the AP2IV-4 locus resulted in the expression of a subset of bradyzoite-specific proteins in replicating tachyzoites that included tissue cyst wall components BPK1, MCP4, CST1 and the surface antigen SRS9. In the murine animal model, the mis-timing of bradyzoite antigens in tachyzoites lacking AP2IV-4 caused a potent inflammatory monocyte immune response that effectively eliminated this parasite and prevented tissue cyst formation in mouse brain tissue. Altogether, these results indicate that suppression of bradyzoite antigens by AP2IV-4 during acute infection is required for *Toxoplasma* to successfully establish a chronic infection in the immune-competent host.

Author summary

The *Toxoplasma* biology that underlies the establishment of a chronic infection is developmental conversion of the acute tachyzoite stage into the latent bradyzoite-tissue cyst stage. Despite the important clinical consequences of this developmental pathway, the molecular basis of the switch mechanisms that control formation of the tissue cyst is still poorly understood. A fundamental feature of tissue cyst formation is the expression of bradyzoite-specific genes. Here we show the transcription factor AP2IV-4 directly silences bradyzoite mRNA and protein expression in the acute tachyzoite stage demonstrating that developmental control of tissue cyst formation is as much about when not to express bradyzoite genes as it is about when to activate them. Losing the suppression of bradyzoite

decision to publish, or preparation of the manuscript.

Competing interests: The authors have declared that no competing interests exist.

gene expression in the acute tachyzoite stage caused by deleting AP2IV-4 blocked the establishment of chronic disease in healthy animals via increased protective immunity suggesting a possible strategy for preventing chronic *Toxoplasma* infections.

Introduction

Toxoplasma gondii is an obligate intracellular parasite that exhibits a multi-host and multi-stage developmental life cycle. Sexual stages are restricted to the gut mucosa of the feline definitive host and asexual stages of the intermediate life cycle occur within any warm-blooded host, including humans. Acute disease is generally asymptomatic in immune-competent hosts, however, primary or recrudescent infection from latent bradyzoites in humans with AIDS, those undergoing chemotherapy or in the unborn cause significant disease and death [1]. While the tachyzoite lytic cycle is responsible for disease pathology in human hosts, the interconversion of the tachyzoite stage into the bradyzoite stage underlies chronic infection and ensures host to host transmission [2]. Evidence indicates that the tachyzoite cell cycle is intricately tied to bradyzoite differentiation with the choice to continue tachyzoite replication or develop into the latent bradyzoite containing tissue cyst made during S phase and/or mitosis [3, 4].

Transcriptome data demonstrates that unique changes in mRNA expression occur in the tachyzoite cell cycle and during development [5–7]. An estimated ~5% of all transcripts are exclusive to a single developmental stage with nearly 40% of the mRNAs in the tachyzoite division cycle periodically expressed. How these changes are controlled is largely unknown. Early genome mining for known gene specific transcription factors revealed two important observations. While the general transcriptional machinery is present in the genomes of Apicomplexa species, initial studies failed to identify classic gene specific transcriptional regulators common to higher eukaryotes. Second, an overall lack of genes encoding DNA binding proteins suggested a limited arsenal from which to regulate these dynamic changes in parasite developmental gene expression. In 2005, a family of DNA binding proteins (ApiAP2 factors) distantly related to the APETALA family plant transcription factors was discovered encoded in the genomes of Apicomplexa species [8]. In *Plasmodium* spp., ApiAP2 factors bind DNA with distinct sequence specificity [9, 10] via a novel domain swapping mechanism [11] and have non-transcriptional roles in sub-telomeric chromosome biology [12]. Examples of ApiAP2 gene-specific functions in *Plasmodium falciparum* are ookinete (AP2-O) and sporozoite (AP2-Sp) ApiAP2s that serve as stage specific transcriptional activators regulating motile stages within the mosquito definitive host [13–15]. Genetic disruption of AP2-O results in non-invasive ookinetes [15] whereas disruption of the AP2-Sp locus yields a parasite unable to form viable sporozoites [14]. The *Toxoplasma* genome encodes 67 ApiAP2 domain-containing proteins (ToxoDB and ref. [16]), with 24 of these genes expressed cyclically during the tachyzoite division cycle [5]. In *Toxoplasma*, ApiAP2s have been implicated in virulence and invasion mechanisms [17], as part of chromatin remodeling complexes [18, 19] and RNA processing machinery [20] and there is evidence for ApiAP2 factors regulating bradyzoite development. AP2XI-4 is up-regulated during bradyzoite development and the loss of AP2XI-4 blocks the stress-induction of some bradyzoite mRNAs, including the canonical marker, BAG1 [21]. The novel stress-inducible transcriptional repressor AP2IX-9 acts to prevent premature commitment to bradyzoite development through direct interaction with bradyzoite specific promoters [22].

Here we describe the discovery of a new level of developmental control in the intermediate life cycle that is required to establish the chronic tissue cyst stage in animals. AP2IV-4 is exclusively expressed in the tachyzoite division cycle with peak expression of the encoded mRNA and protein during early mitosis. Surprisingly, genetic knockouts of AP2IV-4 demonstrate it is non-essential to the replicating tachyzoite but is instead critical for the suppression of bradyzoite surface antigens and cyst wall proteins in the tachyzoite stage. Results from animal studies determined that AP2IV-4 silencing of bradyzoite gene expression is critical to enable tachyzoites to escape an effective immune response and produce the tissue cysts required for transmission.

Results

Many ApiAP2 factors dynamically regulated in the tachyzoite cell cycle are nonessential for growth

Previous studies identified *Toxoplasma* ApiAP2 genes that are cyclically transcribed once per tachyzoite cell cycle with the peak timing of mRNA levels distributed throughout the division cycle [5]. The functions of periodically expressed ApiAP2 factors is largely unknown, although it is proposed they control the remarkable "just-in-time" cell cycle transcriptome of asexual stage Apicomplexa parasites [5, 23]. A Group-of-12 of these periodic ApiAP2 mRNAs share overlapping cyclical profiles that reach maximum expression during the S through mitotic phases (S/M) of the *Toxoplasma* tachyzoite cell cycle (Fig 1A). We made multiple attempts to knockout each of the Group-of-12 ApiAP2 genes (Fig 1B) in a Type I RH strain (RHΔ*ku80*Δ*hxgprt* = RHQ strain) engineered for enhanced homologous recombination [24, 25]. The results from this series of genetic experiments were mixed; half the Group-of-12 ApiAP2 genes were successfully disrupted in the RHQ strain at relatively high prevalence except AP2III-2 (Fig 1B), while knockouts of the other half failed repeated attempts. A recent whole genome CRISPR screen performed in human fibroblast cells (HFF)[26] supports the preliminary RHQ experimental sorting of Group-of-12 ApiAP2 genes into dispensable versus required (Fig 1B, CRISPR column). Alternate developmental expression (and possible function), may help explain why half of the Group-of-12 ApiAP2s are not required for tachyzoite growth. AP2IX-4 [27] and AP2XI-4 [21] are also expressed in bradyzoites and recent studies indicate important roles for these factors in tissue cyst development; similarly AP2III-2, AP2VI-1, and AP2XI-1 are expressed in tachyzoites and bradyzoites [28]. Notably, AP2VI-1 mRNA is expressed at high levels across the *Toxoplasma* intermediate and definitive life cycles (the only ApiAP2 with this profile) and AP2III-2 is highly expressed in unsporulated oocysts [28]. Three of the Group-of 12 ApiAP2 factors that were expressed in tachyzoites and not induced by stress conditions (AP2IV-4, AP2XII-2, AP2XII-9)[28] also failed knockout attempts in RHQ parasites and had significant negative phenotype scores in the HFF/CRISPR study (Fig 1B).

At the mRNA level AP2IV-4 stood out as one of the most dynamic of the Group-of-12 ApiAP2s with a >10-fold change in mRNA abundance over a ~2 h period in the second half of the tachyzoite cell cycle (Fig 1A, red curve). The failure to disrupt AP2IV-4 in RHQ parasites indicated an important function in tachyzoite replication. To verify AP2IV-4 protein is cell cycle regulated, we introduced three copies of the HA epitope tag in frame with the C-terminus of the AP2IV-4 coding region by genetic knock-in, which preserved the native promoter and genomic flanking contexts. The gene model for AP2IV-4 (http://toxodb.org/toxo/app/record/gene/TGME49_318470) predicts a single exon structure that encodes a large protein with a single AP2 DNA binding domain (S1A Fig, diagram), which was verified by Western analysis of AP2IV-4^{HA} expressing parasites (S1A Fig, gel right). As with previously tagged *Toxoplasma*

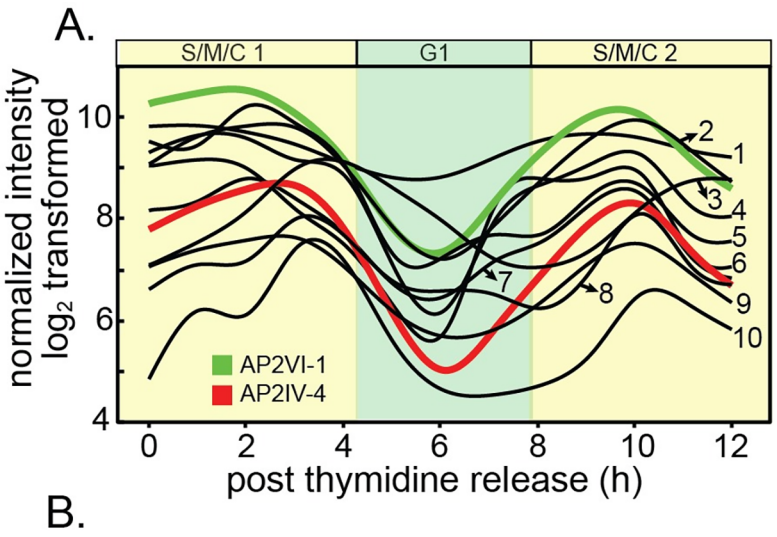

Name	Gene ID TGME49_	KO in RHQ	HFF CRISPR	Results KO/recomb.	Curve #
AP2IX-4	288950	yes	1.92	10/12	4
AP2VI-1	240460	yes	0.69	7/50	green
AP2XI-1	309410	yes	0.55	1/12	5
AP2XI-4	315760	yes	0.29	ref. [21]	3
AP2VIIa-1	280470	failed	0.07	0/140	10
AP2VIIa-8	282210	failed	-0.05	0/96	5
AP2X-11	215570	yes	-0.56	10/12	8
AP2XII-2	217700	failed	-1.16	0/66	6
AP2X-9	215150	failed	-2.29	0/75	1
AP2III-2	253380	yes	-3.22	1/96	2
AP2IV-4	318470	failed	-3.37	0/60	red
AP2XII-9	251740	failed	-4.32	0/75	9

Fig 1. Genetic disruption of S/M regulated ApiAP2 genes. (A.) Shown are the cyclical mRNA profiles of twelve *Toxoplasma* ApiAP2s (Group-of-12) that reach maximum expression in the S phase/mitotic half of the tachyzoite cell cycle (results from our cell cycle transcriptome dataset [5]). All data points are $\log_2$ transformed and gene IDs for the curve numbers are indicated in (B.). AP2IV-4 is one of the most dynamic cyclical ApiAP2 mRNAs (red curve, nontransformed RMA data is minimum 6 h = 21.7 versus maximum 3 h = 433), which peaks during late S phase to early mitosis and is down regulated by the start of G1 phase (see Fig 2). The mRNA encoding AP2VI-1 (green curve) is similarly cell cycle regulated with peak expression slightly earlier than AP2IV-4 **(B.)** Multiple genetic knockout attempts in the RHQ strain were undertaken for eleven of the Group-of-12 ApiAP2 genes (AP2XI-4 knockout results see ref. [21]). Results: number of confirmed knockout clones (KO) versus total drug-resistant recombinants screened by custom PCR is indicated for each Group-of-12 gene. HFF CRISPR: average phenotype score for the Group-of-12 ApiAP2 genes in a recent whole genome CRISPR analysis [26] was included as a reference. In general, negative CRISPR phenotype scores indicate potential greater dependency for tachyzoite growth in HFF cells.

https://doi.org/10.1371/journal.ppat.1007035.g001

ApiAP2s (*e.g.* ref. [5, 22]), AP2IV-4^{HA} in the RHQ strain localized exclusively to the nucleus (Fig 2A) and was cell cycle regulated (Fig 2A and S1B Fig) with a timing similar to its mRNA expression profile (Fig 1A, red curve). In a randomly growing tachyzoite population, AP2IV-4^{HA} was detectable in 30% of vacuoles (S2A and S2B Fig) due to cell cycle periodicity. To pinpoint the exact cell cycle expression of AP2IV-4^{HA}, co-staining with two daughter cytoskeleton markers was utilized to define the timing of initiation, accumulation and degradation of the AP2IV-4^{HA} fusion protein in comparison to the earlier expressing cyclical factor AP2VI-1^{HA} (Fig 1A, green curve) also produced by genetic knock-in. Antibodies for the inner membrane

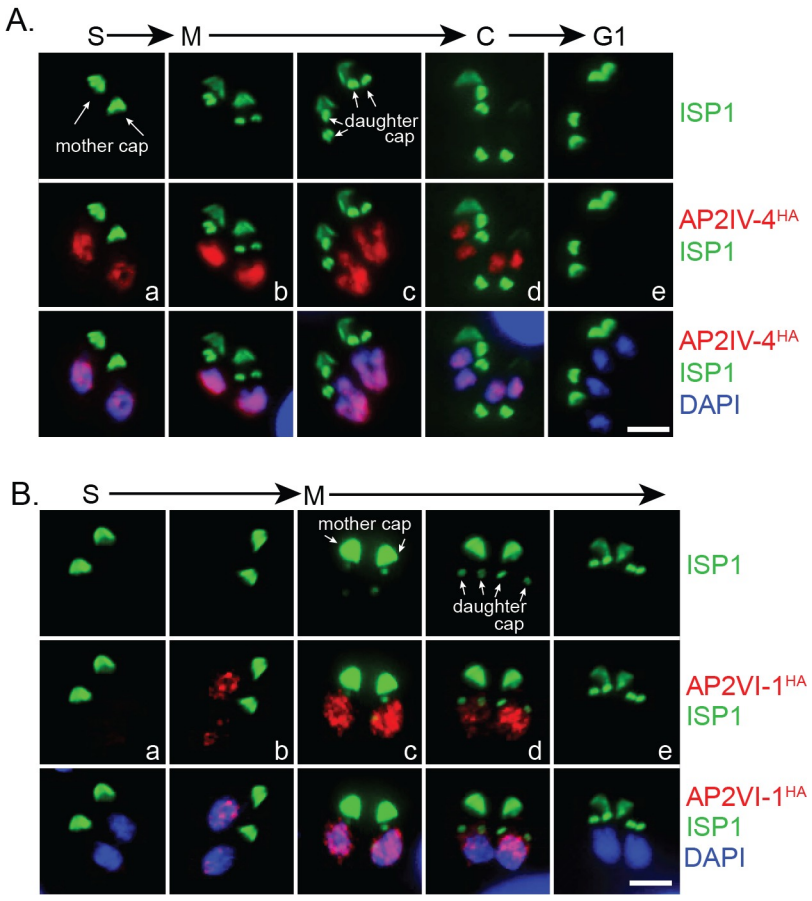

Fig 2. AP2IV-4 is dynamically regulated during the tachyzoite cell cycle. AP2IV-4 and AP2VI-1 were individually C-terminally epitope tagged with 3xHA at the endogenous loci of the RHQ strain by genetic knock-in to preserve native promoter expression. Relative cell cycle progression for each experimental series is indicated above the images. **(A.)** AP2IV-4^{HA} expressing tachyzoites were co-stained with α-ISPI (apical cap, green) and DAPI (DNA, blue,) to determine the exact timing of AP2IV-4^{HA} expression (red) during the tachyzoite cell cycle. Note that intravacuole synchronous expression of AP2IV-4^{HA} and AP2VI-4^{HA} is a characteristic of tachyzoite stage growth. AP2IV-4^{HA} was first detected (image a) prior to daughter ISP1 formation and before the nucleus flattened in late S phase. Maximum AP2IV-4^{HA} protein (b, c) accumulation was marked by the appearance and elongation of daughter apical structures and U-shaped nuclear morphology. As the daughter apical cap (ISP1) matured and nuclear division was completed, AP2IV-4^{HA} disappeared near the end of cytokinesis (d). When all mother apical caps had been resolved and nuclear division completed (G1 phase), AP2IV-4^{HA} was not detectable. Scale bar = 5 μm. **(B.)** AP2VI-1^{HA} parasites were also co-stained with α-ISP1 (apical cap, green) and DAPI (DNA, blue) to pinpoint AP2VI-1^{HA} expression (red) during the tachyzoite cell cycle. Initiation of AP2VI-1^{HA} expression also occurs prior to daughter apical cap formation (b) and achieves peak stabilization as daughter apical cap is formed (c). Apical cap rings (daughter caps, arrows) signify the degradation of AP2VI-1^{HA} expression (d) and AP2VI-1^{HA} is no longer detectable when the apical cap of the internal daughters is mature (e). Nuclear morphology restricts AP2VI-1^{HA} to S phase and early mitosis of the cell cycle, prior to the flattened or U-shaped nucleus of mitosis. Scale bar = 5 μm.

https://doi.org/10.1371/journal.ppat.1007035.g002

complex (S1B Fig, α-TgIMC1)[29] and the apical cap (Fig 2, α-TgISP1) [30] permit the late S phase through mitotic periods of the tachyzoite cell cycle to be resolved in time. AP2IV-4^{HA} first appeared in tachyzoites lacking internal daughter IMC structures as did AP2VI-1^{HA}, although by first AP2IV-4^{HA} detection AP2VI-1^{HA} had already reached maximum expression in these parasites (S1B Fig, a vs. b images). The detection of AP2IV-4^{HA} prior to internal daughter structures indicates initiation of expression in late S phase just prior to the start of mitosis and before nuclear division. The rapid accumulation of AP2IV-4^{HA} paralleled the formation of ISP1 rings of the daughter parasites (Fig 2A, a-c images) and the growth of the

IMC1 daughter scaffold (S1B Fig, c,e images), while during these same cell cycle transitions AP2VI-1^{HA} declined rapidly to undetectable levels (Fig 2B, d,e images; S1B Fig, d,f images). AP2IV-4^{HA} was highly expressed throughout budding (distinct mitotic U-shaped nuclear morphology, DAPI staining, Fig 2A) and began to disappear following nuclear division in late cytokinesis (Fig 2A, images d,e) and was no longer detectable after resolution of the mother IMC, which is consistent with the lack of AP2IV-4 mRNA expression in the G1 phase (Fig 1A).

Expression of AP2IV-4^{HA} in tachyzoites induced to differentiate into bradyzoites by alkaline stress followed a pattern that was consistent with known changes in replication associated with this developmental pathway (S2 Fig)[3]. Alkaline-stress conditions caused AP2IV-4^{HA} parasites to loose intravacular synchronous growth and this led to a heterologous pattern of AP2IV-4^{HA} expression reflective of asynchronous cell cycle distributions in a single vacuole (S2B Fig). However, co-staining alkaline-stressed populations for AP2IV-4^{HA} and centrin, showed that the cell cycle restriction of AP2IV-4 to the second half of the cell cycle was preserved in the differentiating parasites (representative image, S2C Fig). It is challenging to resolve centrosome counts in differentiating populations due to the lack of rosetting and parasite stacking, however, it is clear in the representative example shown that parasites lacking AP2IV-4^{HA} possess a single centrosome. Further, AP2IV-4^{HA} positive parasites are wider than their more slender "vacuolar mates", which is a recognized morphological difference between replicating tachyzoites and dormant mature bradyzoites. Thus, during alkaline-stress induction AP2IV-4^{HA} expression is marking those parasites that are replicating and are likely at an earlier stage in development as growth arrest in the G1 period is the ultimate outcome of this developmental pathway [3, 31, 32]. The expression of AP2IV-4 during early differentiation shares similarities with another of the Group-of-12 cell cycle ApiAP2 factors that we have studied, AP2IX-4 [27].

Successful genetic knockout of AP2IV-4 indicates a nonessential role for tachyzoite growth

The failure to disrupt the AP2IV-4 gene in the RHQ strain (Fig 1B) suggested this factor was essential for tachyzoite growth, although other explanations such as low frequency double crossover or growth defects preventing the recovery of AP2IV-4 knockout parasites could explain the knockout failure. To investigate whether low frequency recombination was responsible, we applied Cre-Lox methods [33] to disrupt AP2IV-4 using the rapamycin-inducible diCRE model recently introduced into the Type I RH*Δhxgprtku80* strain (RHCre)[33]. To "flox" the AP2IV-4 gene in the RHCre strain, we performed serial epitope tagging by genetic knock-in of the AP2IV-4 (3xHA tag) and TGGT1_318480 (3xmyc tag) genes (see Fig 3A diagram), which are in a sequential head to tail configuration on chromosome IV. The AP2IV-4^{HA} fusion protein that resulted from the production of the RHCre-AP2IV-4^{floxed} strain (RHCre-parent in these studies) preserved the native promoter and reproduced the identical 3xHA fusion protein as was generated in the RHQ-AP2IV-4^{HA} strain above (see Fig 2A). Gene TGGT1_318480 is expressed at very low levels in tachyzoites or bradyzoites (<30th mRNA percentile, ToxoDB.org) and was undetectable by both IFA and Western blot following tagging with 3xmyc. Cre-mediated excision of the AP2IV-4 locus was induced by a 6 h incubation with rapamycin (50nM) of RHCre-parent parasites (Fig 3A). In contrast to the failure to knockout AP2IV-4 in the RHQ strain by conventional methods (Fig 1B), ~20% (10/51) of isolated clones following rapamycin treatment of RHCre-parent parasites lacked the AP2IV-4 gene (also no longer HA+), and for two clones we verified the absence of AP2IV-4 mRNA (S3A Fig). The isolation of viable RHCre-*Δap2IV-4* transgenic parasites indicated AP2IV-4 is not essential for tachyzoite growth.

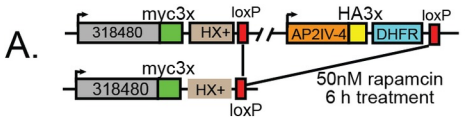

ToxoDB ID TGME49_	RHCre-Parent	RHCre-*Δap2IV-4*	PruQ-Parent	PruQ-*Δap2IV-4*	Description
261650	30.1	517.4	144.3	430.2	unknown
207150	19.8	320.8	224.6	401.8	SRS49C (SAG2D)
280580	59.6	709.7	1046.2	1899.6	SAG4 homolog (SAG4.2)
253330	42.4	455.8	835.1	2315.6	BPK1
320190	23.9	183.6	28.0	256.7	SRS16B (SRS9)
207130	49.0	372.9	171.2	833.7	SRS49A (SAG2Y)
208730	88.8	588.8	249.0	887.6	MCP4
225290	8.3	38.5	24.9	102.4	bradyzoite-NTPase
208740	654.5	2872.4	3657.3	7389.4	microneme protein

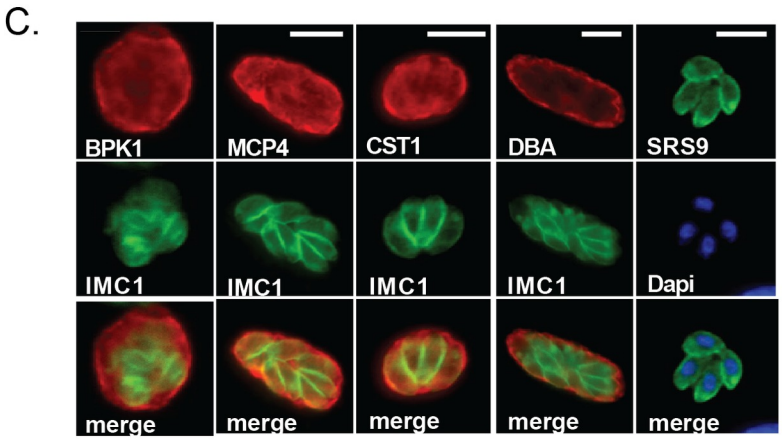

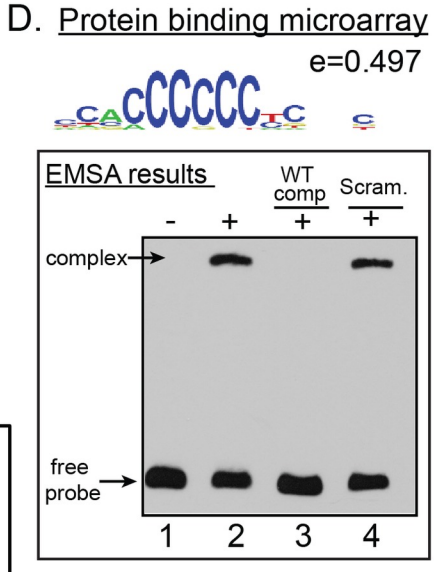

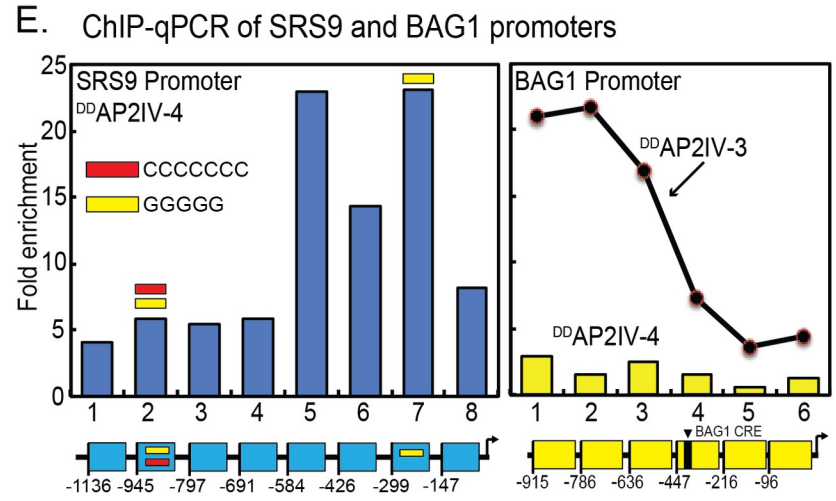

Fig 3. Tissue cyst wall and bradyzoite surface proteins accumulate in tachyzoites lacking AP2IV-4. (A.) Schematic representation of the AP2IV-4 knockout strategy in the RHCre strain. Insertion of loxP sites surrounding the AP2IV-4 locus was accomplished by sequential epitope tagging of TGGT1_318480 and AP2IV-4 genes utilizing the indicated tags and selectable markers. A similar strategy was also used to delete the AP2IV-4 gene in the PruQ-parent strain (S3B Fig). Active Cre-recombinase excises the floxed AP2IV-4 gene in the dual-tagged RHCre and PruQ-strains, which are the parents referred to in this study. Microarray analysis: selected mRNAs altered by the knockout of the AP2IV-4 gene in RHCre- and PruQ-*Δap2IV-4* parasites; average RMA values for RHCre- or PruQ-parent (carrying AP2IV-4^{floxed}) versus *Δap2IV-4* knockout transgenic strains are shown (complete results in S1 Dataset). Note the higher baseline expression of mRNAs in the PruQ- versus the RHCre-parent strains. **(B. and C.)** Average fraction of vacuoles grown under tachyzoite conditions showing DBA+ tissue cyst walls and expression of bradyzoite cyst wall proteins

BPK1, MPC4, CST1 and the bradyzoite-specific surface antigen SRS9 in the PruQ-parent, PruQ-Δ*ap2IV-4* knockout, and PruQ-Δ*ap2IV-4*::AP2IV-4 complemented strains with representative IFA images in (C.) Statistical significance of pairwise parent versus knockout results is indicated (**, $p<0.01$; ***, $p<0.001$). Positive staining for each antigen and DBA+ vacuoles were quantified in triplicate by counting 100 vacuoles from randomly selected microscopic fields. Note also the normal localization of BPK1, CST1, and MCP4 proteins in cyst walls also stained by DBA and the parasite surface localization of SRS9. Unlike bradyzoite heterogenous expression patterns, SRS9 in PruQ-Δ*ap2IV-4* parasites always showed uniform intravacuolar expression consistent with the synchronous replication of tachyzoites. Scale bar = 5 μm. IFA analysis and quantification of these same bradyzoite proteins in RHCre-Δ*ap2IV-4* parasites is presented in supplemental (S4 Fig). **(D.)** To determine whether the single AP2 domain in AP2IV-4 is capable of binding DNA, a protein binding microarray screen was completed using recombinant GST-AP2IV-4 protein (AP2 domain only)(see Material and Methods). The consensus binding sequence from the analysis was determined to be homopolymeric poly(dC):poly(dG); (5'-ACCCCCCT-3'/3'-TGGGGGGA-5'; enrichment score = 0.497) the representative sequence logo shown indicates position weight matrices compiled for each base. An electrophoretic mobility shift assay was completed using 50ng of GST-AP2IV-4 protein and 20 fmol of a 59bp biotinylated DNA probe containing one 6 and one 5 homopolymer poly(dC) stretch (36% total poly(dC) nucleotides). A slowly migrating complex was identified (lane 2, top arrow) that was specifically competed by excess unlabeled poly(dC) competitor DNA (lane 3) but not by excess scrambled DNA fragment containing no more than three consecutive poly(dC) nucleotides (18% poly(dC) nucleotides). **(E.)** ^{DD}AP2IV-4 occupies the native SRS9 promoter in parasite chromatin (see Material and Methods for ChIP-qPCR assay details). Specific ^{DD}AP2IV-4 binding was determined in eight specific regions of the SRS9 promoter 5' to the SRS9 coding region (-1,136 bp flanking including the SRS9 5'-UTR up to the coding ATG). The region of the SRS9 promoter between -584 bp and -192 bp (regions 5–7) showed the highest specific enrichment for ^{DD}AP2IV-4 binding. The occurrence of poly(dC) or poly(dG) motifs (5'-3') in the SRS9 promoter are indicated by red or yellow bars, respectively. ChIP-qPCR analysis of ^{DD}AP2IV-4 binding to the bradyzoite-specific BAG1 promoter in tachyzoite chromatin was included here as a negative control. A previous study established that the stress-induced ApiAP2 activator, AP2IV-3, specifically binds the BAG1 promoter [28] and is shown here only as a positive control reference. Note that the functionally mapped BAG1 CRE [64] is indicated in the included diagram (yellow diagram). All SRS9 and BAG1 primer sets used in the ChIP-qPCR studies are listed in S3 Dataset.

https://doi.org/10.1371/journal.ppat.1007035.g003

Microarray analysis reveals AP2IV-4 controls bradyzoite mRNA expression

Absent a requirement for AP2IV-4 in cell division, it was not clear what role AP2IV-4 serves in the tachyzoite. In order to build clues to understand AP2IV-4 function, duplicate total RNA samples from the RHCre-parent and RHCre-*Δap2IV-4* tachyzoites were isolated (standard tachyzoite conditions, pH 7.0), converted to cRNA and hybridized to a custom *Toxoplasma* Affymetrix GeneChip [34]. In total, 40 mRNAs were altered >2-fold in RHCre-Δ*ap2IV-4* tachyzoites, including 26 mRNAs that were up-regulated (Fig 3A, results of selected genes; complete results in S1 Dataset). Remarkably, the loss of AP2IV-4 caused increased expression of mRNAs encoding known bradyzoite surface antigens (*e.g.* SRS9, SAG4.2) [35, 36] and cyst wall components (*e.g.* BPK1, MCP4)[6, 37] in the tachyzoite. These results indicated the major function for AP2IV-4 is to repress the transcription of key bradyzoite genes in replicating tachyzoites. This new level of developmental control of bradyzoite gene expression in the tachyzoite is distinct from the stress-induced AP2IX-9 mechanism we described previously [22]. Importantly, AP2IV-4 and AP2IX-9 combined appear to transcriptionally silence 66% (14/21, S2 Dataset) of the bradyzoite genes thought to be activated by AP2XI-4 [21], which is also one of Group-of-12 ApiAP2s. The RHCre-*Δap2IV-4* transgenic strain was complemented with the cosmid PSBM794 [38] that carries a *Toxoplasma* genomic DNA fragment spanning the AP2IV-4 gene and RNA samples from the resulting RHCre-*Δap2IV-4*::AP2IV-4 transgenic strain were analyzed on the *Toxoplasma* GeneChip. The results from this experiment determined that reintroduction of the AP2IV-4 gene restored mRNA repression to RHCre-parent levels for >80% of the mRNAs with the remaining mRNAs substantially reduced from the de-repressed levels of RHCre-*Δap2IV-4* tachyzoites (S1 Dataset).

To confirm the function of AP2IV-4 in a second genetic lineage, we employed the same double-tagging strategy to "flox" the AP2IV-4 gene in the Type II Prugniaud strain (PruQ-parent in this study: Pru-Δ*ku80*Δ*hxgprt*/*AP2IV-4*^{floxed})[39] followed by knockout of the AP2IV-4 gene by transient transfection of pMIN-CRE-eGFP plasmid (S3B Fig, diagram)[40]. Two confirmed PruQ-Δ*ap2IV-4* clones lacking the AP2IV-4 gene were recovered from 178 independent clones screened (S3C Fig). The successful disruption of the AP2IV-4 locus in PruQ confirms the dispensability of this factor for tachyzoite growth in a second genetic lineage.

Microarray analysis of PruQ-Δ*ap2IV-4* tachyzoites identified very similar gene expression changes to RHCre-Δ*ap2IV-4* parasites; >90% of genes altered up or down by the loss of AP2IV-4 in these knockout strains were shared (Fig 3A; complete lists S1 Dataset). In the PruQ-Δ*ap2IV-4* parasites, bradyzoite mRNA fold changes were often less than in the RHCre-*Δap2IV-4* tachyzoites due to higher starting baseline levels of mRNA expression in the PruQ-parent strain (Fig 3A and S1 Dataset). Type II Pru strains have significant capacity to spontaneously form bradyzoites [28] and this raised the population baseline expression of bradyzoite mRNAs (Fig 3A, PruQ-parent). Nonetheless, microarray studies of PruQ-Δ*ap2IV-4* parasite mRNA expression clearly validated the conclusion that a major function of AP2IV-4 is to silence bradyzoite surface and cyst wall gene transcription in replicating tachyzoites.

Tachyzoites lacking AP2IV-4 misexpress cyst wall and bradyzoite surface proteins

To verify bradyzoite-specific proteins are expressed in replicating tachyzoites lacking AP2IV-4, we completed immunofluorescence assays (IFA) of PruQ-Δ*ap2IV-4* (Fig 3B and 3C) as well as RHCre-Δ*ap2IV-4* tachyzoites (S4 Fig) using antibodies to four bradyzoite specific proteins (α-BPK1, α-MCP4, α-CST1, α-SRS9) and also evaluated the formation of cyst walls using biotin-labeled *Dolichos biflorus* agglutinin (DBA). Microarray probes for the recently discovered bradyzoite cyst wall protein CST1 [41] were not included in *Toxoplasma* GeneChip, although we suspected the CST1 gene could be a target of AP2IV-4 suppression in tachyzoites. This was confirmed at the mRNA level by RT-qPCR using CST1-specific primers (see S3 Dataset for CST1 primer designs). Staining of PruQ-Δ*ap2IV-4* (Fig 3B and 3C) and RHCre-Δ*ap2IV-4* tachyzoites (S4A Fig) with CST1 antibodies confirmed the mis-timing of expression of this large cyst wall protein (>250 kDa), which was reversed by genetic rescue of these knockout strains with a cosmid genomic clone carrying the AP2IV-4 gene (Fig 3B and S4A Fig). Similar to CST1, the cyst wall pseudokinase BPK1 and structural protein MCP4 as well as bradyzoite surface protein SRS9 were all increased in PruQ- and RHCre-Δ*ap2IV-4* tachyzoites as was the number of DBA+-vacuoles, which was again reversed by genetic complementation (Fig 3B and 3C and S4B and S4C Fig). In comparison to alkaline-induced PruQ-parental bradyzoites, PruQ-Δ*ap2IV-4* tachyzoites expressed the bradyzoite mRNAs and proteins shown here within a normal range expected of bradyzoites and the proteins were properly localized to either cyst walls or the parasite surface (Fig 3C, see also S4B Fig). The, expression of bradyzoite-specific genes in the Δ*ap2IV-4* tachyzoites of either strain was the result of developmental mis-timing. Type I RH parasites are known to be resistant to developmental induction [42], and therefore, it was remarkable that deletion of a single ApiAP2 factor could accomplish what strong alkaline stress fails to do in this strain. The expression of bradyzoite-specific antigens in Δ*ap2IV-4* populations was not 100% for either strain, which likely reflects the restricted S/M cell cycle window that AP2IV-4 operates (Figs 1 and 2). Intriguingly, we reported previously that increased baseline bradyzoite mRNA expression occurs during the S/M periods of synchronized tachyzoites [5]. This hypothesis was examined further by co-staining PruQ-Δ*ap2IV-4* and PruQ-parent tachyzoites with α-SRS9 and α-centrin antibodies (S5A Fig). This IFA analysis determined that the majority of SRS9+/PruQ-Δ*ap2IV-4* parasites possessed duplicated centrosomes (S/M phases) confirming that SRS9 misexpression was occurring primarily in the mitotic half of the tachyzoite cell cycle. Similarly, most of the 14.3% of PruQ-parental parasites that spontaneously expressed SRS9 also possessed duplicated centrosomes (only 3% of parental parasites were in the G1 phase and also SRS9+). Altogether, these results are consistent with the unique relationship between bradyzoite differentiation and tachyzoite mitosis that we discovered more than a decade ago [3].

AP2IV-4 binds DNA with sequence specificity

ApiAP2 factors have been shown to regulate gene expression through the binding of target promoters in a sequence specific manner [9, 10, 12, 14, 15, 17, 22]. To assess DNA binding specificity for AP2IV-4, a GST-AP2IV-4 fusion protein (AP2 domain only) was expressed, purified and incubated on a microchip containing all possible 10-mer DNA fragments (Fig 3D, protein binding microarray results). A resulting 8-nucleotide "consensus" sequence motif bound specifically by the GST-AP2IV-4 fusion protein contains homopolymeric poly(dC):poly(dG) (Fig 3D, 5'-ACCCCCCT-3'/3'-TGGGGGGA-5'; enrichment score 0.497). Electrophoretic mobility shift assays (EMSA) using DNA probes containing poly(dC):poly(dG) repeats were used to validate the specificity of GST-AP2IV-4 binding (Fig 3D, EMSA results) [22]. GST-AP2IV-4 bound biotin-labeled DNA probes that contained a single instance of the "consensus" PBM motif and a second five nucleotide poly(dC) segment (Fig 3D, lane 2), and was successfully competed using 300x excess unlabeled poly(dC) competitor DNA (Fig 3D, lane 3), but not with unlabeled DNA probes that contained no poly(dC) stretch greater than three nucleotides (Fig 3D, lane 4). In a larger protein binding screen of 46 *Toxoplasma* AP2 domains, two other ApiAP2 factors, AP2VIIa-5 and AP2XII-4, were determined to also specifically bind homopolymeric poly(dC):poly(dG) DNA (Kim et al, in preparation). In addition, a recent analysis of nucleosome-free regions for enriched DNA motifs discovered poly(dC):poly(dG) repeats were preferentially found upstream of cell cycle and bradyzoite genes, such as SRS9 (Wang et al, in preparation).

The presence of poly(dC):poly(dG) repeats in the SRS9 promoter (Fig 3E, blue legend) suggested AP2IV-4 might directly bind this promoter. To examine this question, we utilized the FKBP (DD)/Shield 1 conditional expression model [43] in order to improve the signal strength for AP2IV-4 expression, which has been very successful for studying ApiAP2 factors in *P. falciparum* and *Toxoplasma* [13, 22, 44]. The FKBP peptide combined with three copies of the HA epitope tag was fused to the N-terminus of the AP2IV-4 coding region (^{DD}AP2IV-4) by genetic knock-in methods. The addition of Shield 1 (100nM) to RHQ-^{DD}AP2IV-4 transgenic parasites successfully increased nuclear levels of ^{DD}AP2IV-4, but did not disrupt the normal periodic cell cycle expression of this protein. Thus, there are likely significant post-transcriptional mechanisms regulating AP2IV-4 expression in tachyzoites as we also previously documented for AP2IX-9 expression [22]. Utilizing lysates prepared from RHQ-^{DD}AP2IV-4 tachyzoites incubated with Shield 1, we performed chromatin immunoprecipitation followed by quantitative PCR of eight regions covering ~1,200bp of the SRS9 promoter and 5'-UTR (Fig 3E). The results from this experiment showed that binding of ^{DD}AP2IV-4 to the SRS9 promoter in parasite chromatin was enriched in regions 5–7 that includes a poly(dG) motif (region 7, yellow bar) ~230bp upstream of the SRS9 ATG (Fig 3E). To control for non-specific binding, we analyzed ^{DD}AP2IV-4 binding to the chromosome region (-950 bp) 5'-flanking of the BAG1 bradyzoite gene. In contrast to stress-induced AP2IV-3, which we have recently reported activates BAG1 [28], AP2IV-4 does not regulate BAG1 (S1 Dataset). No enrichment of ^{DD}AP2IV-4 binding was detected to the six regions tested within the BAG1 promoter (Fig 3E), whereas ^{DD}AP2IV-3 binding to this promoter is significantly enriched [28] (Fig 3E, reference line graph).

The loss of AP2IV-4 prevents tissue cyst formation in vivo

Our results indicated that PruQ-Δ*ap2IV-4* parasites are tachyzoites expressing a few genes that are normally induced to high levels during bradyzoite development. Unlike bradyzoites (S2B and S2C Fig), RHCre- and PruQ-Δ*ap2IV-4* tachyzoites replicated synchronously within a shared vacuole, which is a growth behavior observed for all native tachyzoite strains. PruQ-

Δ*ap2IV-4* parasites also retained normal SAG1 surface antigen expression even as they also expressed bradyzoite-specific surface antigen, SRS9 (S5B Fig). Finally, whole-cell mRNA analysis of PruQ-parent and PruQ-Δ*ap2IV-4* tachyzoites revealed nearly identical transcriptomes (S5C Fig), whereas, the transcriptomes of native Type II tachyzoites and bradyzoites have numerous differences and lower quantitative similarity (S5C Fig).

RHCre-Δ*ap2IV-4* tachyzoites are a Type I strain and consistent with the limited number of genes regulated by AP2IV-4 the knockout of this gene did not disrupt the lethality of the Type I genetic background. Inoculation (i.p) of BALB/c mice with 500 RHCre-Δ*ap2IV-4* (or RHCre-parent) parasites was fully lethal, while infections with a very high dose ($1x10^7$) of PruQ-Δ*ap2IV-4* parasites was not (Fig 4A). These data are consistent with the known difference in the virulence of Type I versus II strains, and while the PruQ-parent strain showed slightly higher virulence (LD100 $>10^6$) this difference was minor compared to the acute virulence of RHCre strains lacking AP2IV-4. By contrast, the loss of AP2IV-4 had a dramatic effect on PruQ-strain chronic infections in mice. Shifting PruQ-Δ*ap2IV-4* parasites into alkaline media (pH8.2) effectively slowed growth and induced high levels of DBA+ tissue cysts (Fig 4B, in vitro = 93.1%) demonstrating PruQ-Δ*ap2IV-4* parasites were capable of forming cysts in vitro. However, PruQ-Δ*ap2IV-4* infections of BALB/c mice failed to produce tissue cysts in brain tissue (Fig 4B). The lack of tissue cyst formation was correlated with a lower parasite burden measured in BALB/c mice at 6 days post-inoculation (Fig 4C), although lower parasite burden was not due to an inability of PruQ-Δ*ap2IV-4* parasites to replicate in vivo. Mice infected intraperitoneally with PruQ-Δ*ap2IV-4* display no reduction in the frequency of infection or growth as compared to the PruQ-parent or the complemented strain at day one post infection (Fig 4D and S6A Fig), which is in agreement with the lack of any growth difference of these strains in HFF cell culture. This indicates that PruQ-Δ*ap2IV-4* parasites efficiently invade host cells and replicate productively early in the infection, but as the infection progresses the parasites that lack AP2IV-4 are more effectively eliminated by the immune response of BALB/c mice.

Mis-timing of bradyzoite protein expression in tachyzoites recruits an effective host immune response

The development of bradyzoites and cysts in vivo is, at least partly, dependent upon immune factors. This is illustrated in immune deficient animals where bradyzoites fail to develop and mice succumb due to uncontrolled tachyzoite replication. The protective immune response during acute infection is dominated by the recruitment of inflammatory monocytes and T cell production of IFN-γ [45]. During chronic infection, IFN- γ is required to prevent parasite recrudescence. Yet, the host immune response is unable to clear the bradyzoite and cysts persist for long periods in host tissues. The pay off between protection and the development of chronic infection is poorly understood. At day 6 post *Toxoplasma* infection neutrophils and inflammatory monocytes, distinguished by their expression of Ly6 surface antigens and distinct morphologies (Fig 5A and 5B), are present at the site of infection. Although neutrophils are important sources of IL-12, inflammatory monocytes are the key effector cell in controlling parasite replication [46]. Analysis of the proportion of these populations following infection of parasites with an intact or disrupted AP2IV-4 gene revealed striking differences. Consistent with the response to a high inoculum of parasites [46], infection with the PruQ-parent induced the influx of neutrophils, outweighing inflammatory monocytes nearly 3-fold (Fig 5A, 5B and 5D). By contrast, PruQ-Δ*ap2IV-4* infections at day 6 post-infection led to a significant increase in the proportion of inflammatory monocytes (Fig 5A) that was not observed early in the infection (S6A Fig). This was confirmed by cytospin, where large numbers of polymorphonuclear neutrophils can be seen in the peritoneal exudate wash of mice infected with PruQ-

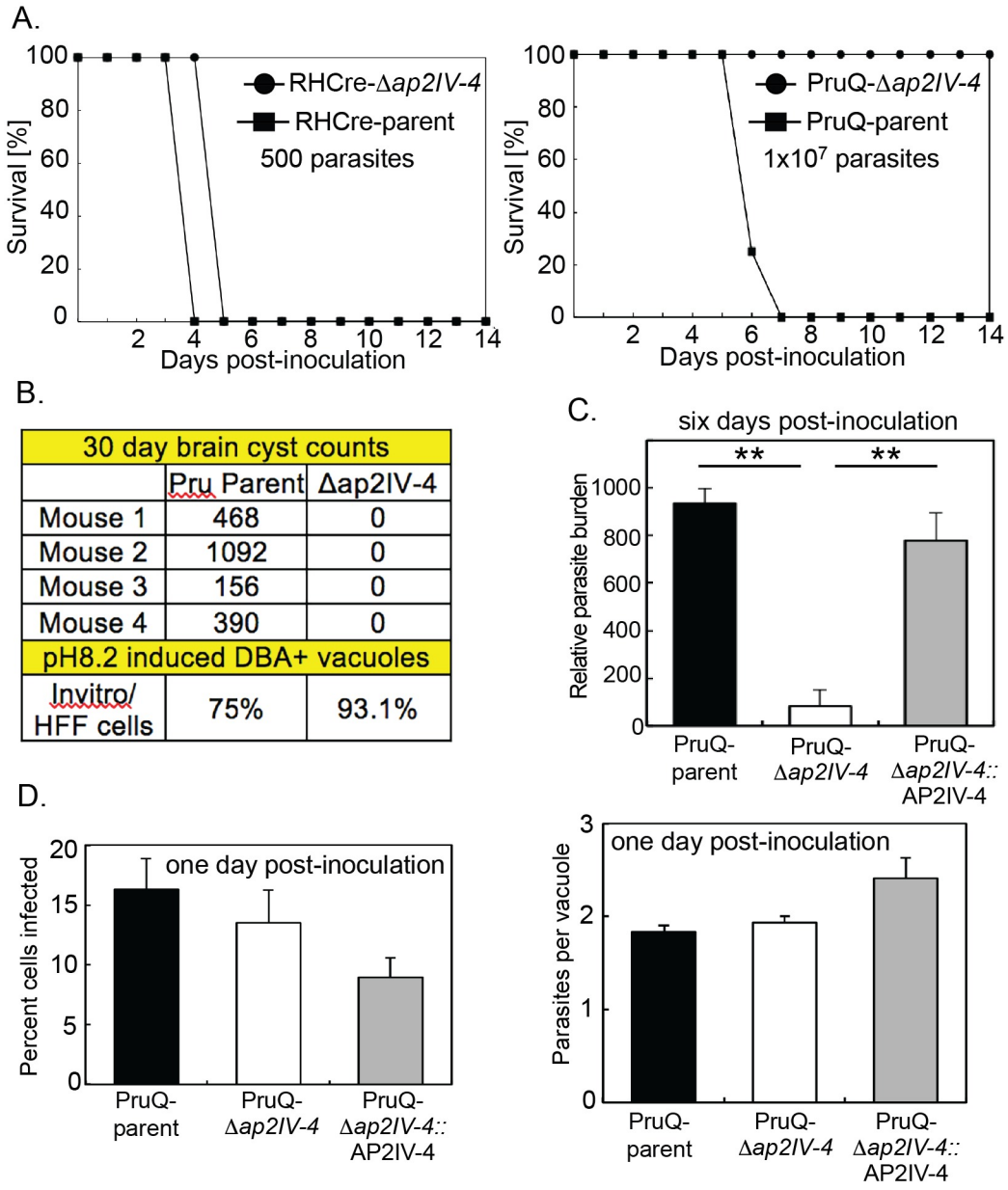

30 day brain cyst counts		
	Pru Parent	Δap2IV-4
Mouse 1	468	0
Mouse 2	1092	0
Mouse 3	156	0
Mouse 4	390	0
pH8.2 induced DBA+ vacuoles		
Invitro/ HFF cells	75%	93.1%

Fig 4. Loss of AP2IV-4 affects the establishment of chronic disease in mice. (A.) Inoculation (i.p.) of BALB/c mice with AP2IV-4 knockout strains; PruQ-Δ*ap2IV-4* or RHCre-Δ*ap2IV-4* and parental PruQ- or RHCre-strains recapitulates the acute virulence of Type I versus relative avirulence of the Type II genetic background. RHCre-strain infection dose = 500 parasites, PruQ-strain infection dose = $1x10^7$ parasites. Note that all mice survive an infection with $1x10^6$ or lower dose of PruQ-parent parasites for at least 30 days (see B.), while mice did not survive the $1x10^7$ dose indicating PruQ-Δ*ap2IV-4*, parasites are slightly more avirulent than the matched parent strain. **(B.)** PruQ-Δ*ap2IV-4* parasites were induced by alkaline-stress (72 h, pH 8.2 media) to form tissue cysts (DBA+) at high levels in HFF cells, whereas, these parasites were unable to form tissue cysts in brain tissue of BALB/c mice compared to the PruQ-parent strain. Tissue cysts numbers in mice were determined at 30 day post-infection. **(C.)** At six-days post infection, total DNA was extracted from peripheral tissues and parasite burden for PruQ-parent, PruQ-Δ*ap2IV-4*, and PruQ-Δ*ap2IV-4*:AP2IV-4 strain-infections determined following amplification of the B1 gene compared against a standard curve. Statistical significance (*, $p<0.05$) is indicated. **(D.)** BALB/c mice were inoculated intraperitoneally with $1x10^7$ parasites of either PruQ-parent, PruQ-Δ*ap2IV-4*, or PruQ-Δ*ap2IV-4*:AP2IV-4 strains. At day one post-infection peritoneal cells were harvested and spun onto cytospin slides. Slides were stained using HEMA3 staining kit and examined under a light microscope. The infection frequency and parasite vacuole size was determined in triplicate. Note that there is no significant difference in the infection frequency for any of these strains at the early timepoint post-infection (see also S6A Fig).

https://doi.org/10.1371/journal.ppat.1007035.g004

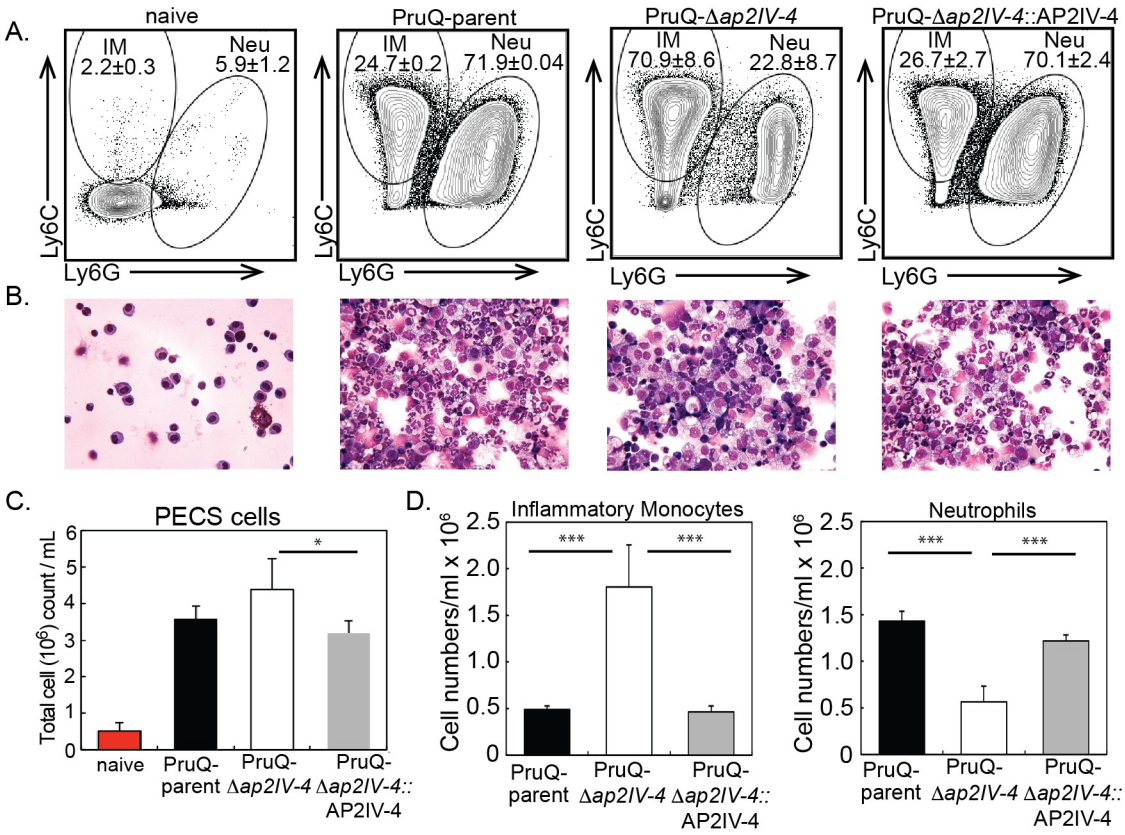

Fig 5. Infection with PruQ-Δ*ap2IV-4* tachyzoites preferentially recruits inflammatory monocytes. (A.) Peritoneal exudate cells were harvested at day six post-infection from mice inoculated with either PruQ-parent, PruQ-Δ*ap2IV-4*, or PruQ-Δ*ap2IV-4*:AP2IV-4 strains and subjected to immunostaining for flow cytometry. Cells were stained for extracellular antigens, and gated on CD45 + cells for analysis. Inflammatory monocytes ($Ly6C^{hi}$, $Ly6G^{neg}$) and neutrophils ($Ly6C^{int}$ $Ly6G^{hi}$) were determined and averaged **(B.)** Representative cytospin images are provided immediately below the matching FACS plots. **(C.)** Total cell infiltration into the peritoneum of infected mice. Cell counts were quantified based on volume recovered from the peritoneal wash. **(D.)** Absolute cell quantification of inflammatory monocytes and neutrophils. Data are representative of a minimum of 4 individual experiments and 5 mice per group. Statistical significance (*, $p<0.05$; **, $p<0.01$) is indicated.

https://doi.org/10.1371/journal.ppat.1007035.g005

parental parasites and foamy monocytes observed with PruQ-Δ*ap2IV-4* parasite infection (Fig 5B). Further, the absolute numbers of inflammatory monocytes recruited to the site of infection is greater in the absence of AP2IV-4 with a corresponding decrease in the recruitment of neutrophils (Fig 5C and 5D). Although PruQ-Δ*ap2IV-4* parasites can be found replicating in peritoneal exudate cells, cytospin counts suggest that overall, the proportion of inflammatory monocytes infected with this strain is highly reduced at day 6 post-infection (S6B Fig). Genetic complementation of the PruQ-Δ*ap2IV-4* parasites restored the innate immune response to that of mice infected with the PruQ-parent (Fig 5 and S6B Fig). Together, these data indicate that in the absence of AP2IV-4 silencing of bradyzoite gene expression in the tachyzoite stage, there is an amplification of the protective innate immune response driven by inflammatory monocytes.

Discussion

The life cycle of *Toxoplasma* is heteroxenous with a sexual definitive cycle in the felid host and a second intermediate life cycle in any endothermic animal including humans. The steps of the intermediate life cycle leading to tissues cysts in murine brain tissue illustrate this

developmental process [4]. Bradyzoite/sporozoite oral infection leads to population wide development of the tachyzoite stage [47, 48] that is followed by systemic spread of tachyzoites. In particular, spread into the vasculature resulting in the infection of endothelial cells of brain capillaries is a critical route for tachyzoites to cross the BBB into the brain [49]. Through poorly understood mechanisms, the tachyzoites slow growth [4] and alter their transcriptome to form dormant bradyzoite-tissue cysts in neurons [50] setting the stage for transmission to the next host animal. Thus, there are two competing demands of the *Toxoplasma* intermediate life cycle; expand tachyzoite numbers to ensure systemic spread within a host [49] and produce the dormant bradyzoite-tissue cyst required for passing the infection onto a new host [4]. How *Toxoplasma* mechanistically balances these competing demands is not understood. However, clues are emerging from our studies of ApiAP2 factors (see Fig 6 model). Early bradyzoite development is associated with the induction of six *Toxoplasma* ApiAP2 genes (AP2Ib-1, AP2IV-3, AP2VI-3, AP2VIIa-1, AP2VIII-4, AP2IX-9) that are not expressed in the tachyzoite [22, 28]. Remarkably, these factors do not operate in the same direction. AP2IX-9, is a stress-inducible repressor of bradyzoite gene expression [22], while AP2IV-3 is a stress-induced transcriptional activator (and likely AP2Ib-1) regulating many of the same bradyzoite genes as AP2IX-9 [28]. The studies here add unexpected new complexity to bradyzoite developmental gene expression. AP2IV-4 was the first transcription factor expressed in replicating tachyzoites whose major function is the regulation of tissue cyst formation. Thus, our studies have uncovered a complex ApiAP2 transcriptional network of repressors and activators competing at the interface of tachyzoite replication and early switching to regulate tissue cyst formation (see Fig 6 model). Notably, we have not yet identified an ApiAP2 that exclusively operates late in bradyzoite development. For the ApiAP2 gene family, the most distinguishing feature of mature bradyzoites is the down regulation of many ApiAP2 factors [28].

Does the lack of ApiAP2 factors specific for mature bradyzoites mean that once initiated bradyzoite development in vivo progresses to maturity? Answering this question will be challenging given the asynchrony of bradyzoite development. However, a recent analysis of tissue cyst biology provides two important insights; tissue cyst size in the infected murine brain is related to tachyzoite vacuole size at the time of switching and average cyst numbers in tissues like murine brain become stable after an early period [28]. Add to this the observation that tissue cyst recrudescence is rare in the brain of immune-competent animals [51], returns the

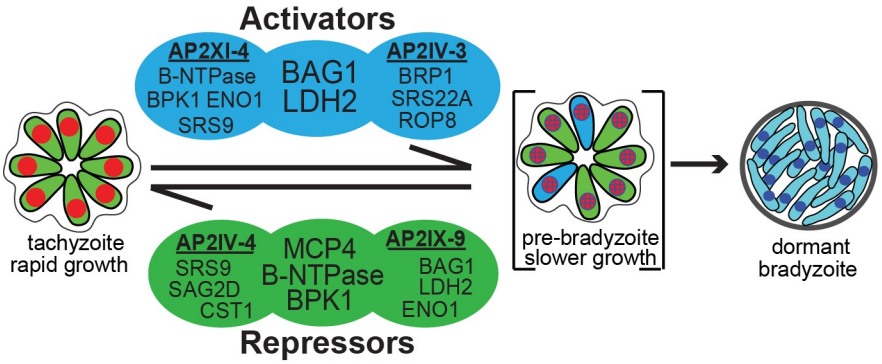

Fig 6. ApiAP2 transcriptional network controlling bradyzoite development. Transcriptional activators AP2XI-4 [21] and AP2IV-3 [28] co-regulate BAG1 and LDH2 genes and independently regulate other bradyzoite genes (representative genes shown, see S2 Dataset for complete gene lists). Similarly, transcriptional repressors AP2IV-4 and AP2IX-9 [22] regulate common (B-NTPase, MCP4, BPK1) and independent sets of bradyzoite genes. Note, AP2XI-4 and AP2IV-4 are Group-of-12 cell cycle ApiAP2s of tachyzoites (Fig 1), while AP2IV-3 and AP2IX-9 are stress-inducible factors not expressed in replicating tachyzoites [22, 28].

https://doi.org/10.1371/journal.ppat.1007035.g006

discussion to the critical importance of the tachyzoite stage for fulfilling the biotic demands of the intermediate life cycle. The discovery of AP2IV-4 highlights the concept that specific life cycle decisions begin upstream in the developmental pathway and provides insight into the mechanisms that link the tachyzoite cell cycle to bradyzoite development. Together, the cell cycle AP2IV-4 and the stress-inducible AP2IX-9, comprise two independent levels of transcriptional regulation preventing bradyzoite development in *Toxoplasma*. This is convincing support for the hypothesis that tachyzoite growth is the primary driver of parasite biomass and through dissemination the tachyzoite finds suitable host cell environments for which to develop ultimately end-stage bradyzoites [4, 22]. In addition, the overlap of gene regulatory targets between AP2IV-4 and AP2IX-9 (S2 Dataset) indicate there is some redundancy governing the induction of the bradyzoite developmental pathway indicating the importance of preventing premature commitment to the bradyzoite stage that leads to dormancy [22]. The earliest clues to unfolding bradyzoite development in *Toxoplasma* revolves around the central role asexual stage replication plays in the transition to growth-arrested end-stages [3, 31, 52]. DNA replication in the tachyzoite is required for bradyzoite development [52] and the tachyzoite is "poised" to enter the bradyzoite developmental pathway during each round of replication [3]. The sub-transcriptome of the tachyzoite S and mitotic phases is enriched in basal bradyzoite transcripts [5] and developing populations have more 2N parasites [3], which is a cell cycle timing that corresponds with peak AP2IV-4 expression. This places AP2IV-4 perfectly within the tachyzoite cell cycle to regulate these critical developmental processes. Repressing tissue cyst wall formation in the tachyzoite could provide the parasite with flexibility to maintain a replicative stage or quickly interpret "development" signals in the animal resulting in induction of bradyzoite differentiation when the parasite encounters the immune system and/or a tissue that favors tissue cyst longevity. In addition to controlling when and where tissue cyst formation occurs, repressors like AP2IV-4 may need to be re-expressed for pre-bradyzoites or bradyzoites to recrudesce. Consistent with this idea, our previous studies demonstrated bradyzoites from murine brain cysts re-express tachyzoite antigens prior to their first division in HFF cells and most bradyzoites that failed to re-express them did not divide [3].

These studies also demonstrate that deletion of a single ApiAP2 factor in *Toxoplasma* can significantly alter the course of the host immune response. Thus, host influences on ApiAP2 evolution has likely led to mechanisms that suppress bradyzoite antigens during acute infection, which we show here is required to establish a chronic infection in the murine brain. There are implications from this discovery for future vaccine development that might block tissue cyst formation in food animals, and thereby eliminate this source of human infections, which is an unmet therapeutic challenge. Our results point to inflammatory monocytes as a major component of the immune response contributing to protective immunity in the absence of AP2IV-4 (Fig 5) [45, 53]. A rapid response to the signature of a fast replicating lytic parasite is appropriate but there would be little evolutionary drive to respond equivalently to a slow replicating cyst form. Thus, changing the signatures of the parasite as we have done here with the deletion of AP2IV-4 have dramatically altered the early immune response, with bradyzoite antigens now being seen in the context of significant cell lysis. Increased inflammatory monocyte recruitment may point to a change in the ability of the parasite to be seen by the innate immune response. This could be either increased TLR recognition of bradyzoite antigens or a failure to inhibit signaling pathways by the tachyzoite. Perhaps predictably in the presence of enhanced monocyte recruitment, the T cell response is also superior, and the adaptive immune response to these parasites will be of significant interest in future studies. Alternatively, the mis-timing of bradyzoite antigen expression in the replicating and systemic tachyzoites lacking AP2IV-4 may increase the overall function of the immune response by either targeting it more

rapidly to the bradyzoite or act as an adjuvant to the overall anti-parasite response. Further studies will be needed to fully understand the molecular mechanism(s) responsible for the shift to a more protective immune response. It is worth noting that the functions now emerging for AP2IV-4 in controlling in vivo persistence were not uncovered by cell culture models. Achieving bradyzoite switching in vitro in the mid-90's was a major breakthrough, and much has and will be learned using these models [54, 55]. However, the complexity of parasite encounters with host cells and tissues in animals cannot be replicated by these models. Distinct tissue tropisms observed for tissue cyst formation in animals infected with *Toxoplasma* [47, 56–58] suggest the parasite senses different host cell environments and relays this information to the mechanisms controlling developmental switching [4]. We know little about the molecular basis for *Toxoplasma* host tissue tropisms, however, it is likely that the network of ApiAP2 repressors and activators we have discovered will have critical roles in these host-parasite interactions.

Materials and methods

A summary analysis of the AP2IV-4 microarray data can be found in S1 Dataset. For a comparative analysis of genes regulated by AP2IV-3, AP2XI-4, AP2IV-4 and AP2IX-9, please see S2 Dataset. All new gene expression data sets produced in this study have been uploaded to the Gene Expression Omnibus (GSE93531). All transgenic strains and oligonucleotides used in this study are found in S3 Dataset

Cell culture, genetic manipulation and conditional genome engineering

Toxoplasma tachyzoites were serially passaged in vitro using confluent tissue culture flasks ($T25cm^2$ and $T175cm^2$) containing human foreskin fibroblasts (HFF cells; obtained from ATCC, Manassas, VA).

Conventional ApiAP2 knockouts. To create ApiAP2 gene replacement plasmids for Group-of-12 factors (Fig 1), the 5' UTR and 3'UTR regions (>500bp each flank) were PCR amplified from RH genomic DNA and cloned via the BP reaction into pDONRP4-P1R or pDONRP2R-P3, respectively. The pDONRP1-P2 plasmid containing the HXGPRT selectable marker is described [59]. Finally, the three entry plasmids (5'ApiAP2 UTR:HXGPRT:3'ApiAP2) were combined in the LR reaction with pDESTP4-P3 to create the expression plasmid pDEST"ApiAP2" HXGPRT KO. All BP and LR reactions were done according to manufacturer's protocol (Thermo Fisher); 25μg of pDEST"ApiAP2" HXGPRT KO plasmid was transfected into $2.5x10^7$ RHQ tachyzoites then parasites were selected in media supplemented with xanthine (40μg/ml) and mycophenolic acid (50μg/ml). When drug resistant parasites were observed, clones were isolated by limiting dilution.

Introduction of loxP recognition sites. loxP recognition sites were introduced by inverse PCR amplification of the pLIC-3xHA/DHFR and pLIC-3xmyc/HXGPRT plasmids, followed by ApaI digestion of the linear PCR product and T4 DNA ligation to re-circularize the plasmid. This resulted in the introduction of a loxP site downstream of the indicated *T. gondii* selectable marker (ex. Fig 3A), creating the plasmids pLIC3xmyc/HXGPRT/loxP and pLIC-3xHA/DHFR/loxP. *Toxoplasma* gene TGGT1_318480 was fused with a triple repeat of the myc3 epitope in RHCre or PruQ by homologous recombination using the pLIC3xmyc/HXGPRT/loxP plasmid. Likewise, AP2IV-4 (TGGT1_318470) was fused with a triple HA epitope in clonal isolates of RHCre-318480^{myc} or PruQ-318480^{myc} by homologous recombination with the pLIC-3xHA/DHFR/loxP plasmid, thereby "floxing" the AP2IV-4 genomic locus. Rearrangement of the genetic locus of interest was verified by nested PCR for all clones isolated. Please see S3 Dataset for strain details and oligonucleotide sequences.

CRE-recombinase expression. Expression of CRE-recombinase strain was induced in RHCre-AP2IV-4^{floxed} parasites as previously described [33]. To initiate CRE mediated excision of AP2IV-4, RHCre-AP2IV-4^{floxed} parasites were seeded at a 5:1 MOI in HFF monolayers, allowed to invade for 2 h, washed 3x with Hanks balanced salt solution (Corning) to remove all free floating parasites and followed by 6 h treatment with 50nM rapamycin. The monolayers were scraped, twice passaged through a 25ga needle, filtered to remove host debris and immediately cloned by limiting dilution to reduce competition from the background of "wild type" AP2IV-4 parasites. For PruQ-AP2IV-4^{floxed}, 5x10^7 parasites were transfected with 25μg of pMIN-CRE-eGFP plasmid [40], allowed to recover for 24 h, scraped, force lysed by passage through a 25ga needle, filtered and immediately cloned by limiting dilution.

Cosmid complementation. Cosmid isolates that span the AP2IV-4 locus were identified with the gBrowse function at www.ToxoDB.org. PSBM794 was selected and 10μg of cosmid DNA was transfected into 1x10^7 RHCre-Δ*ap2IV-4* or PruQ-Δ*ap2IV-4* parasites and a stable population selected using two rounds of phleomycin (5mg/ml for 10 h, followed by sustained 5μg/ml) selection.

Conditional expression of AP2IV-4. The AP2IV-4 (TGGT1_318470) coding sequence was PCR amplified from RH genomic DNA with oligonucleotides that included in-frame MfeI/EcoRV sites, which were used to clone the PCR fragment into the pCTDDHA3x plasmid (Dr. Boris Striepen, University of Georgia). The resulting plasmid, pCTDDHA3x-AP2IV-4, contains an N-terminal fusion of the FKBP peptide (11.2 kDa) and a triple repeat of the HA epitope (4.4 kDa) fused in-frame with AP2IV-4 (^{DD}AP2IV-4) that allows for ectopic conditional expression of the fusion protein using the small molecule Shield 1 [22]. The plasmid was transfected into the RHQ strain and transgenic parasites selected using chloramphenicol (20 μM) with individual clones isolated by limiting dilution.

Endogenous epitope fusions with 3xHA. *Toxoplasma* genes AP2IV-4 (TGGT1_318470) and AP2VI-1 (TGGT1_240460) were tagged at the genomic locus with a triple copy of HA in RHQ by homologous recombination using the pLIC-3xHA/DHFR plasmid as previously described [25].

Immunofluorescence assays and Western analysis

Parasites were grown in confluent HFF cells and prepared for immunofluorescence as previously described [60]. Primary antibodies were used at the following concentrations: HA (rat mAb 3F10, 1:500, Roche); ISP1 (mouse mAb clone 7E8, 1:2000, Dr. Peter Bradley, University of California, Los Angeles); IMC1 (mouse mAb, 1:1000, Dr. Gary Ward, University of Vermont); biotin-labeled *Dolichos biflorus* agglutinin (DBA) (Vector labs, CA,1:3000); BPK1, MCP4 and SAG1 (mouse polyclonal antibodies = pAbs, 1:1000, Dr. John Boothroyd, Stanford University,); CST1 (mouse pAb, Salmon E, 1:2000, Dr. Louis Weiss, Albert Einstein College of Medicine); SRS9 (rabbit pAb, 1:1000, Dr. Laura Knoll, University of Wisconsin). Secondary antibodies by Alexa or streptavidin conjugated secondary antibodies were used at a 1:1000 dilution. All images were collected with a Zeiss Axiovert microscope equipped with 100x objective. Statistical significance was calculated using the one-tailed t-test, p values as indicated.

Protein from 25x10^6 parasites were isolated, purified and whole parasite lysates collected as previously described [60] and subjected to electrophoresis on a SDS-PAGE gel. After transfer to nitrocellulose, the blots were probed with primary antibodies for CST1 (mouse pAb, Salmon E, 1:2000, Dr. Louis Weiss, Albert Einstein College of Medicine) and the loading control TgNF3 (mouse pAb, 1:1000, Dr. Stan Tomavo, Pasteur Institute, Lille)[61]. Detection of the proteins was completed using HRP conjugated antibodies (Jackson ImmunoResearch) followed by chemiluminescence reaction for visualization.

RNA microarray

Two independent biological replicates of total RNA were isolated from five RHCre transgenic strains (S3 Dataset): RHCre-AP2IV-4^{floxed} clone ID6 (RHCre-parent), RHCre-Δ*ap2IV-4* clones 27 and 30, and cosmid complemented populations (PSBM794; RHCre-Δ*ap2IV-4*::AP2IV-4) of each knockout. Likewise, two biological replicates were isolated from the following PruQ strain transgenics (3 total strains): PruQ-AP2IV-4^{floxed} clone C3 (PruQ-parent), PruQ-Δ*ap2IV-4* clones 10 and 34. RNA quality for all strains was evaluated using the Agilent Bioanalyzer 2100 (Santa Clara, CA) and 500ng of total RNA was prepared for hybridization on the ToxoGeneChip as described [5]. The resulting data was analyzed using GeneSpring GX software (v11.5, Agilent) and all microarray data made available in the Gene Expression Omnibus (GSE93531).

Protein expression and electrophoretic mobility shift assay (EMSA)

The AP2 domain (amino acids 782–854) of AP2IV-4 was cloned into pGEX4T3 and expressed as a GST-fusion protein. Following affinity purification on a glutathione column, purified GST-AP2IV-4 protein was subjected to protein binding microarrays as previously described [9, 22]. Complementary oligonucleotides were annealed to create 5'-biotinylated DNA probes of 59bp (WT) and 60bp (scrambled). All binding reactions contained 20fmol DNA probe and 50ng of GST-AP2IV-4 protein. Non-biotinylated "cold" competitor probe was added at 300x concentration. GST-AP2IV-4-DNA complexes were resolved on a 6% polyacrylamide PAGE gel, transferred to a nylon membrane and interactions visualized using the LightShift Chemiluminescent EMSA kit as described by the manufacturer (Thermo Fisher, Waltham, MA). Oligonucleotide sequences used for GST-AP2IV-4 expression and DNA probes can be found in S3 Dataset.

Chromatin immunoprecipitation and qPCR

Chromatin immunoprecipitation followed by quantitative PCR (ChIP-qPCR) was performed as previously published (supplement of ref. [22]). In brief, RH-^{DD}AP2IV-4 and RHΔ*hxgprt* (negative control) parasites were inoculated at 3:1 MOI in T175 cm^2 flasks, allowed to invade for 1 h, rinsed three times with Hanks balanced salt solution (Gibco) to remove free floating parasites and fresh media containing 100nM Shield 1 was added. Parasite cultures were allowed to grow 36 h prior to intracellular crosslinking with formaldehyde and isolation of nuclear fraction. Nuclear material was subjected to sonication to shear DNA into 200-1000bp fragments and soluble fraction incubated with α-HA antibody (5μg, ab9110, rabbit, Abcam). Protein-DNA complexes were isolated using protein-G coupled magnetic beads (Dynabeads, Invitrogen) and DNA isolated by treatment with 1% SDS followed by phenol-chloroform extraction and ethanol precipitation. Whole genome amplification (Sigma-Aldrich) was performed on ChIP-DNA and purified by Qiagen Mini-Elute PCR kit. qPCR was performed using 20ng/rxn of specific (^{DD}AP2IV-4) chromatin and non-specific chromatin (RHΔ*hxgprt*) using Fast SYBR green master mix on an ABI7900 according to manufacturer's protocols. Relative enrichment was calculated with the equation: $2^{\wedge-(\Delta Ct\ target-\Delta Ct\ non\text{-}target)}$ where the change in Ct value of specific versus nonspecific chromatin at the SRS9 and BAG1 promoters was calculated. All ChIP-qPCR oligonucleotides used can be found in S3 Dataset.

Animals and infections

Mice were purchased from Jackson or Harlan Laboratories. 10–12 week old BALB/c mice were infected with 1x10^7 PruQ-parental strain or PruQ-Δ*ap2IV-4* intraperitoneally in sterile PBS.

Uninfected, age-matched mice were used as naïve uninfected controls. Mice were monitored daily and euthanized at day one and day six-post infection for study.

To examine acute virulence and tissue cyst formation, 5–6 week old female BALB/c mice were injected intraperitoneally with 10^5, 10^6, or 10^7 PruQ-parent or PruQ*Δap2IV-4* parasites (4 mice per group, 10^7 dose only shown in Fig 4). Plaque assays were performed for each sample and ensured equal viability between strains. Mice were examined daily and time to death was recorded. Serology performed on cardiac bleeds of infected mice confirmed presence of *Toxoplasma*. To assess cyst burden, BALB/c mice were infected with $1x10^6$ parasites as described above and allowed to progress to chronic infection for 30 days (4 mice per group). Brains were then homogenized; homogenates were fixed, quenched, and permeabilized. Samples were blocked in 3% BSA/1xPBS/0.2% Triton X-100. To visualize cyst walls, rhodamine-conjugated *Dolichos biflorus* lectin (Vector Labs) was applied at 1:250 dilution overnight at 4˚C. Cyst quantification was performed as previously described [62].

Cell collection and flow cytometry

Following euthanasia, peritoneal exudate cells (PECs) were collected from the peritoneal cavity in sterile PBS. Cells were counted using an automated cell counter, and total cell numbers were determined using the volume recovered from the peritoneum. Aliquots were used for cytospins, and stained using HEMA3 stains. For flow cytometry, cells were incubated with 1:10 FC Block (BD, 553142) for 5 minutes on ice, and subsequently incubated with fluorophore-conjugated antibodies to CD45, CD11b, CD11c, Ly6C, Ly6G. Cells were washed, resuspended in FACS buffer and samples acquired using a BD FACS Canto II flow cytometer. Analysis was conducted using Flowjo software.

Parasite burden

Peripheral tissues were placed in tissue lysis buffer for DNA isolation. DNA was isolated using a genomic DNA purification kit (Roche, 11796828001). To quantify parasite burden, quantitative PCR (Bioline) was conducted on isolated DNA by amplification of the *Toxoplasma* B1 gene (F: 5' TCCCCTCTGCTGGCGAAAAGT 3' R: 5' AGCGTTCGTGGTCAACTATCG 3'). Parasite burden was quantified using a standard curve as previously described [63].

Ethics statement

All animal research was conducted in accordance with the animal welfare act, and all protocols were approved by the Institutional Animal Care and Use Committees at the University of California, Riverside (approved protocol #A-20140007) or the Indiana University School of Medicine (approved protocol #10852).

Supporting information

S1 Dataset. Complete microarray results for all gene expression altered by knockout of AP2IV-4 in PruQ and RHCre strains.
(XLSX)

S2 Dataset. Comparison of genes controlled by AP2IV-3, AP2IV-4, AP2IX-9, and AP2XI-4.
(XLSX)

S3 Dataset. Full list of transgenic strains and oligonucleotides used in this study.
(XLSX)

S1 Fig. AP2IV-4 and AP2VI-1 expression during daughter budding. (A.) The AP2IV-4 single exon and AP2 domain gene is predicted to encode a ~250kDa protein (http://toxodb.org/toxo/app/record/gene/TGME49_318470), which was confirmed by Western analysis (α-HA) of AP2IV-4^{HA} parasites (plus 3xHA, actual protein size is ~254kDa). Molecular mass standards indicated on the left. **(B.)** IFA analysis of AP2IV-4^{HA} and AP2VI-1^{HA} transgenic parasites grown in HFF monolayers utilized co-stains α-HA (green, AP2IV-4^{HA} or AP2VI-1^{HA} expression) and α-IMC1 (black and white panels). To improve visualization of internal bud structures, IMC1 images were decolorized and then inverted. AP2IV-4^{HA} and AP2VI-1^{HA} are exclusively localized to the nucleus and the relative cell cycle expression profile predicted by the cyclical mRNA patterns (Fig 1A, green and red curves) was confirmed for each factor. Black scale bar = 5 μm.
(TIF)

S2 Fig. Developmental expression of AP2IV-4. (A.) Representative microscope field showing two vacuoles of PruQ-AP2IV-4^{HA} parasites; one vacuole is synchronously expressing AP2IV-4^{HA}, while the other is negative for this factor due to the cell cycle regulation of AP2IV-4 expression. IFA analysis utilized co-stains α-HA (red, AP2IV-4^{HA}) and α-IMC1 (green). **(B.)** Quantification of AP2IV-4^{HA} expression in tachyzoites and alkaline-shifted bradyzoites at the times indicated. 100 randomly selected vacuoles stained with α-HA (red, AP2IV-4^{HA}) and DBA were counted in triplicate. Tissue cysts (DBA+) that were also positive for AP2IV-4^{HA} were sorted into five bins based on the fraction of AP2IV-4^{HA} positive parasites. IFA images showing representative patterns of AP2IV-4^{HA} expression in the tissue cysts from each of the five bins (cell cycle marker IMC1 and AP2IV-4^{HA} co-stains) is shown below the graph. **(C.)** Representative image of a differentiating vacuole (72 h post-alkaline shift) co-stained with α-centrin (centrosome) and α-HA (AP2IV-4^{HA}). Note the distinct morphology of the two AP2IV-4^{HA} parasites that possessed a duplicated centrosome adjacent to the nucleus, which are likely mitotic. In contrast to the uniform centrin staining in the AP2IV-4^{HA}-positive parasites, centrin staining in the AP2IV-4^{HA}-negative parasites varied in intensity and composition with many parasites containing a faint, single dot of centrin.
(TIF)

S3 Fig. Genetic knockout strategy for AP2IV-4. (A.) Verification of AP2IV-4 knockout by RT-PCR in the RHCre-Δ*ap2IV-4* transgenic clones. AP2IV-4 mRNA is detected in lane P (parent strain, RHCre-AP2IV-4^{floxed}), but absent from both AP2IV-4 knockout clones evaluated (RHCre-Δ*ap2IV-4* clones 27, and 30). For a diagram of the RHCre knockout strategy see Fig 3A. Complementation for the loss of AP2IV-4 in RHCre-Δ*ap2IV-4* parasites was accomplished using cosmid PSBM794, which reintroduces a full copy of the AP2IV-4 gene and restores AP2IV-4 mRNA expression (C lanes). **(B.)** Diagram of the AP2IV-4 knockout strategy in Type II PruQ-parent (AP2IV-4^{floxed}), which is similar to the knockout of AP2IV-4 in the RHCre strain (see Fig 3A). Here transient transfection of pMIN-CRE-eGFP plasmid into the PruQ-AP2IV-4^{floxed} strain was required to introduce active Cre recombinase. **(C.)** PruQ-parent (lane P) expresses the expected AP2IV-4 transcript, whereas PruQ-Δ*ap2IV-4* clones 10 and 34 (lanes Δ10 and Δ34) lack the AP2IV-4 mRNA. AP2IV-4 cDNA primers amplify a 1367bp fragment of the single exon gene (7221bp full length). For loading and template quality control, GAPDH primers were designed around a 432bp intron, allowing detection of both mRNA (202bp, intron spliced out) and contaminating genomic DNA (634 bp). The absence of a detectable 634bp amplicon in all samples indicates the RNA templates were free of genomic DNA contamination. See S3 Dataset for all primer designs.
(TIF)

S4 Fig. Deletion of the AP2IV-4 gene in the RHCre strain leads to de-repression of bradyzoite surface and cyst wall mRNAs and proteins in the tachyzoite stage. (A.) RHCre-parent (AP2IV-4^{floxed}, open bar), -Δ*ap2IV-4* knockout (black bar), and -Δ*ap2IV-4*::AP2IV-4 complemented (grey bar) parasites were grown in HFF cells for 24 h under standard tachyzoite culture conditions (pH 7.0) and then IFA analysis performed using α-IMC1 (green stain, tachyzoite replication marker) and antibodies to cyst wall protein, CST1 (red stain). Scale bar = 5 μm. CST1 positive vacuoles in each strain were quantified in triplicate by counting 100 vacuoles in randomly selected microscopic fields (**, $p<0.01$). Increased expression of CST1 protein in two independent RHCre-Δ*ap2IV-4* clones (Δ clones, see also S3A Fig) compared to the RHCre-parental (P = AP2IV-4^{floxed}) strain revealed by Western analysis. Nucleolar TgNF3 (43kDa) protein was included as a loading control. Protein mass markers 230kDa and 50 kDa on left. Immunofluorescence images included on right are representative of CST1 positive vacuoles showing cyst wall localization in RHCre-Δ*ap2IV-4* parasites. **(B.)** Representative IFA images of RHCre-Δ*ap2IV-4* tachyzoites expressing bradyzoite-specific proteins BPK1 and MCP4 with normal localization at the periphery of the vacuole consistent with DBA+ cyst wall structures, likewise expression of bradyzoite-specific SRS9 in the RHCre-Δ*ap2IV-4* tachyzoites was properly localized to the parasite surface. Note the uniform intravacuolar expression of SRS9 in RHCre-Δ*ap2IV-4*. Scale bar = 5 μm. **(C.)** Numbers of BPK1, MPC4, DBA, and SRS9 positive vacuoles in RHCre-parent, RHCre-Δ*ap2IV-4* and RHCre-Δ*ap2IV-4*:AP2IV-4 tachyzoites. Statistical significance indicated (**, $p<0.01$; ***, $p<0.001$). Positive staining vacuoles for each strain were quantified in triplicate by counting 100 vacuoles in randomly selected microscopic fields.
(TIF)

S5 Fig. AP2IV-4 knockout parasites retain dominant tachyzoite phenotypes. (A.) The cell cycle distribution of SRS9+ parasites in PruQ-Δ*ap2IV-4* versus the PruQ-parent strains was determined by IFA analysis with αSRS9 and αCentrin (centrosome marker) antibodies. Representative PruQ-Δ*ap2IV-4* co-stained images demonstrate the association of SRS9 expression with parasites containing duplicated centrosomes (S/M/C phases) that was quantified and graphed for PruQ-Δ*ap2IV-4* and the PruQ-parent strains. All parasite counts were determined in triplicate from 100 vacuoles selected at random. The association of SRS9+ expression in S phase and mitotic PruQ-Δ*ap2IV-4* parasites (duplicated centrosome) versus G1 phase (single centrosome) parasites was statistically significant ($p<0.001$). Scale bar = 5 μm. **(B.)** The tachyzoite nature of SRS9+ PruQ-Δ*ap2IV-4* parasites was confirmed by IFA analysis with αSRS9 and αSAG1 antibodies. The expression of SRS9 in PruQ-Δ*ap2IV-4* parasites was nearly ~50% (as shown in A.), and thus, about half the population was SAG1+/SRS9- (#1 vacuole of four parasites circled). Nearly all PruQ-Δ*ap2IV-4* parasites expressing SRS9+ were also positive for SAG1+ surface expression (representative vacuole #3 circled). The fraction of SAG1+ positive vacuoles in PruQ-parent and PruQ-Δ*ap2IV-4* (SRS9- and SRS9+) infected HFF cell cultures were quantified (see graph). In rare examples, PruQ-Δ*ap2IV-4* parasites that were SRS9+ also showed diminished SAG1 expression (#2 vacuole circled). Scale bar = 5 μm **(C.)** Whole-cell mRNA analysis of Type II PruQ-Δ*ap2IV-4* parasites. The analysis of total mRNA expression of PruQ-Δ*ap2IV-4* versus PruQ-parent parasites grown under tachyzoite conditions shows nearly complete identity (r = 0.984) with the exception of the few mRNAs altered by the loss of AP2IV-4 (Fig 3A and S1 Dataset). Note mRNAs misexpressed by the loss of AP2IV-4 have higher levels in the PruQ-Δ*ap2IV-4* parasites, while few tachyzoite mRNAs are downregulated. A reference plot for native Type II strain (M4 isolate) differences (r = 0.786) in developmental mRNA expression of tachyzoites versus bradyzoites is shown. Type II M4 strain data was obtained from the GEO repository (accession #GSE32427). Type II PruQ-parent and PruQ-

Δ*ap2IV-4* mRNA data is also deposited in GEO (accession #GSE93531). The mRNA levels for SRS9, MCP4, and BPK1 are indicated by the indicated colored circles in each plot. AP2IV-4 mRNA levels (red circle) are only indicated in the PruQ plot. All mRNA expression data was $\log_2$ transformed.
(TIF)

S6 Fig. PruΔ*ap2IV-4* parasites infect equivalently to the PruQ-parent and complemented strains at day one, but are mostly absent by day 6 post-infection. (A.) Peritoneal exudate cells were collected at one day post-infection with 10^7 tachyzoites intraperitoneally. Cells from the peritoneal wash were spun onto cytoslides and stained hematologically. Representative images at both 25X and 63X are provided. Representative parasite vacuoles are marked by a (*). **(B.)** Cytospins of peritoneal washes from animals six days post-infection were harvested and stained as above. Percentages of infected monocytes and polymorphonuclear neutrophils were determined by microscopy.
(TIF)

Acknowledgments

T. gondii genomic and/or cDNA sequence data were accessed via http://ToxoDB.org. The authors would like to thank Drs. Elena Suvorova, Olivier Lucas, Kami Kim, Louis Weiss, and Manuel Llinas for their insights and contributions that helped this paper come together. We especially thank Dr. Erandi K. De Silva for her expertise in generating protein binding microarray results. All gene *Toxoplasma* GeneChip expression data was generated by the Moffitt Cancer Center Molecular Genomics core facility.

Author Contributions

Conceptualization: Joshua B. Radke, William J. Sullivan, Jr., Emma H. Wilson, Michael W. White.

Data curation: Joshua B. Radke, David Hong.

Formal analysis: Joshua B. Radke, Danielle Worth, David Hong, William J. Sullivan, Jr., Emma H. Wilson, Michael W. White.

Funding acquisition: Emma H. Wilson, Michael W. White.

Investigation: Joshua B. Radke, Danielle Worth, David Hong, Sherri Huang.

Project administration: Michael W. White.

Supervision: William J. Sullivan, Jr., Emma H. Wilson, Michael W. White.

Validation: Danielle Worth, David Hong, Sherri Huang.

Writing – original draft: Joshua B. Radke, Emma H. Wilson, Michael W. White.

Writing – review & editing: Joshua B. Radke, Danielle Worth, David Hong, Sherri Huang, William J. Sullivan, Jr., Emma H. Wilson, Michael W. White.

References

1. Luft BJ, Remington JS. Toxoplasmic encephalitis in AIDS. Clin Infect Dis. 1992; 15(2):211–22. Epub 1992/08/01. PMID: 1520757.
2. Montoya JG, Liesenfeld O. Toxoplasmosis. Lancet. 2004; 363(9425):1965–76. Epub 2004/06/15. https://doi.org/10.1016/S0140-6736(04)16412-X PMID: 15194258.

3. Radke JR, Guerini MN, Jerome M, White MW. A change in the premitotic period of the cell cycle is associated with bradyzoite differentiation in Toxoplasma gondii. Mol Biochem Parasitol. 2003; 131(2):119–27. Epub 2003/09/27. PMID: 14511810.
4. White MW, Radke JR, Radke JB. Toxoplasma development—turn the switch on or off? Cell Microbiol. 2014. Epub 2014/01/21. https://doi.org/10.1111/cmi.12267 PMID: 24438211.
5. Behnke MS, Wootton JC, Lehmann MM, Radke JB, Lucas O, Nawas J, et al. Coordinated progression through two subtranscriptomes underlies the tachyzoite cycle of Toxoplasma gondii. PLoS One. 2010; 5(8):e12354. Epub 2010/09/25. https://doi.org/10.1371/journal.pone.0012354 PMID: 20865045; PubMed Central PMCID: PMC2928733.
6. Buchholz KR, Fritz HM, Chen X, Durbin-Johnson B, Rocke DM, Ferguson DJ, et al. Identification of tissue cyst wall components by transcriptome analysis of in vivo and in vitro Toxoplasma gondii bradyzoites. Eukaryot Cell. 2011; 10(12):1637–47. Epub 2011/10/25. https://doi.org/10.1128/EC.05182-11 PMID: 22021236; PubMed Central PMCID: PMC3232729.
7. Radke JR, Behnke MS, Mackey AJ, Radke JB, Roos DS, White MW. The transcriptome of Toxoplasma gondii. BMC Biol. 2005; 3(1):26. https://doi.org/10.1186/1741-7007-3-26 PMID: 16324218.
8. Balaji S, Babu MM, Iyer LM, Aravind L. Discovery of the principal specific transcription factors of Apicomplexa and their implication for the evolution of the AP2-integrase DNA binding domains. Nucleic Acids Res. 2005; 33(13):3994–4006. Epub 2005/07/26. https://doi.org/10.1093/nar/gki709 PMID: 16040597; PubMed Central PMCID: PMC1178005.
9. Campbell TL, De Silva EK, Olszewski KL, Elemento O, Llinas M. Identification and genome-wide prediction of DNA binding specificities for the ApiAP2 family of regulators from the malaria parasite. PLoS Pathog. 2010; 6(10):e1001165. Epub 2010/11/10. https://doi.org/10.1371/journal.ppat.1001165 PMID: 21060817; PubMed Central PMCID: PMC2965767.
10. De Silva EK, Gehrke AR, Olszewski K, Leon I, Chahal JS, Bulyk ML, et al. Specific DNA-binding by apicomplexan AP2 transcription factors. Proc Natl Acad Sci U S A. 2008; 105(24):8393–8. Epub 2008/06/11. doi: 0801993105 [pii] https://doi.org/10.1073/pnas.0801993105 PMID: 18541913; PubMed Central PMCID: PMC2423414.
11. Lindner SE, De Silva EK, Keck JL, Llinas M. Structural determinants of DNA binding by a P. falciparum ApiAP2 transcriptional regulator. J Mol Biol. 2010; 395(3):558–67. Epub 2009/11/17. https://doi.org/10.1016/j.jmb.2009.11.004 PMID: 19913037; PubMed Central PMCID: PMC2813365.
12. Flueck C, Bartfai R, Niederwieser I, Witmer K, Alako BT, Moes S, et al. A major role for the Plasmodium falciparum ApiAP2 protein PfSIP2 in chromosome end biology. PLoS Pathog. 2010; 6(2):e1000784. Epub 2010/03/03. https://doi.org/10.1371/journal.ppat.1000784 PMID: 20195509; PubMed Central PMCID: PMC2829057.
13. Kafsack BF, Rovira-Graells N, Clark TG, Bancells C, Crowley VM, Campino SG, et al. A transcriptional switch underlies commitment to sexual development in malaria parasites. Nature. 2014; 507(7491):248–52. https://doi.org/10.1038/nature12920 PMID: 24572369; PubMed Central PMCID: PMCPMC4040541.
14. Yuda M, Iwanaga S, Shigenobu S, Kato T, Kaneko I. Transcription factor AP2-Sp and its target genes in malarial sporozoites. Mol Microbiol. 2010; 75(4):854–63. Epub 2009/12/23. https://doi.org/10.1111/j.1365-2958.2009.07005.x PMID: 20025671.
15. Yuda M, Iwanaga S, Shigenobu S, Mair GR, Janse CJ, Waters AP, et al. Identification of a transcription factor in the mosquito-invasive stage of malaria parasites. Mol Microbiol. 2009; 71(6):1402–14. Epub 2009/02/18. doi: MMI6609 [pii] https://doi.org/10.1111/j.1365-2958.2009.06609.x PMID: 19220746.
16. Altschul SF, Wootton JC, Zaslavsky E, Yu YK. The construction and use of log-odds substitution scores for multiple sequence alignment. PLoS computational biology. 2010; 6(7):e1000852. Epub 2010/07/27. https://doi.org/10.1371/journal.pcbi.1000852 PMID: 20657661; PubMed Central PMCID: PMC2904766.
17. Walker R, Gissot M, Huot L, Alayi TD, Hot D, Marot G, et al. Toxoplasma transcription factor TgAP2XI-5 regulates the expression of genes involved in parasite virulence and host invasion. J Biol Chem. 2013; 288(43):31127–38. Epub 2013/09/13. https://doi.org/10.1074/jbc.M113.486589 PMID: 24025328; PubMed Central PMCID: PMC3829425.
18. Saksouk N, Bhatti MM, Kieffer S, Smith AT, Musset K, Garin J, et al. Histone-modifying complexes regulate gene expression pertinent to the differentiation of the protozoan parasite Toxoplasma gondii. Mol Cell Biol. 2005; 25(23):10301–14. https://doi.org/10.1128/MCB.25.23.10301-10314.2005 PMID: 16287846.
19. Wang J, Dixon SE, Ting LM, Liu TK, Jeffers V, Croken MM, et al. Lysine acetyltransferase GCN5b interacts with AP2 factors and is required for Toxoplasma gondii proliferation. PLoS Pathog. 2014; 10(1):e1003830. Epub 2014/01/07. https://doi.org/10.1371/journal.ppat.1003830 PMID: 24391497; PubMed Central PMCID: PMC3879359.

20. Braun L, Cannella D, Ortet P, Barakat M, Sautel CF, Kieffer S, et al. A complex small RNA repertoire is generated by a plant/fungal-like machinery and effected by a metazoan-like Argonaute in the single-cell human parasite Toxoplasma gondii. PLoS Pathog. 2010; 6(5):e1000920. Epub 2010/06/05. https://doi.org/10.1371/journal.ppat.1000920 PMID: 20523899; PubMed Central PMCID: PMC2877743.

21. Walker R, Gissot M, Croken MM, Huot L, Hot D, Kim K, et al. The Toxoplasma nuclear factor TgAP2XI-4 controls bradyzoite gene expression and cyst formation. Mol Microbiol. 2013; 87(3):641–55. Epub 2012/12/18. https://doi.org/10.1111/mmi.12121 PMID: 23240624; PubMed Central PMCID: PMC3556193.

22. Radke JB, Lucas O, De Silva EK, Ma Y, Sullivan WJ Jr., Weiss LM, et al. ApiAP2 transcription factor restricts development of the Toxoplasma tissue cyst. Proc Natl Acad Sci U S A. 2013; 110(17):6871–6. Epub 2013/04/11. https://doi.org/10.1073/pnas.1300059110 PMID: 23572590; PubMed Central PMCID: PMC3637731.

23. Bozdech Z, Llinas M, Pulliam BL, Wong ED, Zhu J, DeRisi JL. The transcriptome of the intraerythrocytic developmental cycle of Plasmodium falciparum. PLoS Biol. 2003; 1(1):E5. Epub 2003/08/21. https://doi.org/10.1371/journal.pbio.0000005 PMID: 12929205; PubMed Central PMCID: PMC176545.

24. Fox BA, Ristuccia JG, Gigley JP, Bzik DJ. Efficient gene replacements in Toxoplasma gondii strains deficient for nonhomologous end joining. Eukaryot Cell. 2009; 8(4):520–9. https://doi.org/10.1128/EC.00357-08 PMID: 19218423; PubMed Central PMCID: PMCPMC2669201.

25. Huynh MH, Carruthers VB. Tagging of endogenous genes in a Toxoplasma gondii strain lacking Ku80. Eukaryot Cell. 2009; 8(4):530–9. Epub 2009/02/17. https://doi.org/10.1128/EC.00358-08 PMID: 19218426; PubMed Central PMCID: PMC2669203.

26. Sidik SM, Huet D, Ganesan SM, Huynh MH, Wang T, Nasamu AS, et al. A Genome-wide CRISPR Screen in Toxoplasma Identifies Essential Apicomplexan Genes. Cell. 2016; 166(6):1423–35 e12. https://doi.org/10.1016/j.cell.2016.08.019 PMID: 27594426; PubMed Central PMCID: PMCPMC5017925.

27. Huang S, Holmes MJ, Radke JB, Hong DP, Liu TK, White MW, et al. Toxoplasma gondii AP2IX-4 Regulates Gene Expression during Bradyzoite Development. mSphere. 2017; 2(2). https://doi.org/10.1128/mSphere.00054-17 PMID: 28317026; PubMed Central PMCID: PMCPMC5352832.

28. Hong DP, Radke JB, White MW. Opposing Transcriptional Mechanisms Regulate Toxoplasma Development. mSphere. 2017; 2(1). https://doi.org/10.1128/mSphere.00347-16 PMID: 28251183; PubMed Central PMCID: PMCPMC5322347.

29. Mann T, Beckers C. Characterization of the subpellicular network, a filamentous membrane skeletal component in the parasite Toxoplasma gondii. Mol Biochem Parasitol. 2001; 115(2):257–68. Epub 2001/06/23. PMID: 11420112.

30. Beck JR, Rodriguez-Fernandez IA, de Leon JC, Huynh MH, Carruthers VB, Morrissette NS, et al. A novel family of Toxoplasma IMC proteins displays a hierarchical organization and functions in coordinating parasite division. PLoS Pathog. 2010; 6(9):e1001094. Epub 2010/09/17. https://doi.org/10.1371/journal.ppat.1001094 PMID: 20844581; PubMed Central PMCID: PMC2936552.

31. Jerome ME, Radke JR, Bohne W, Roos DS, White MW. Toxoplasma gondii bradyzoites form spontaneously during sporozoite- initiated development. Infect Immun. 1998; 66(10):4838–44. PMID: 9746587.

32. Radke JR, Streipen B, Guerini MN, Jerome ME, Roos DS, White MW. Defining the cell cycle for the tachyzoite stage of Toxoplasma gondii. Mol Biochem Parasitol. 2001; 115(2):165–75. PMID: 11420103

33. Andenmatten N, Egarter S, Jackson AJ, Jullien N, Herman JP, Meissner M. Conditional genome engineering in Toxoplasma gondii uncovers alternative invasion mechanisms. Nat Methods. 2013; 10(2):125–7. Epub 2012/12/25. https://doi.org/10.1038/nmeth.2301 PMID: 23263690; PubMed Central PMCID: PMC3605914.

34. Bahl A, Davis PH, Behnke M, Dzierszinski F, Jagalur M, Chen F, et al. A novel multifunctional oligonucleotide microarray for Toxoplasma gondii. BMC Genomics. 2010; 11:603. Epub 2010/10/27. doi: 1471-2164-11-603 [pii] https://doi.org/10.1186/1471-2164-11-603 PMID: 20974003; PubMed Central PMCID: PMC3017859.

35. Kim SK, Boothroyd JC. Stage-specific expression of surface antigens by Toxoplasma gondii as a mechanism to facilitate parasite persistence. J Immunol. 2005; 174(12):8038–48. Epub 2005/06/10. PMID: 15944311.

36. Kim SK, Karasov A, Boothroyd JC. Bradyzoite-specific surface antigen SRS9 plays a role in maintaining Toxoplasma gondii persistence in the brain and in host control of parasite replication in the intestine. Infect Immun. 2007; 75(4):1626–34. Epub 2007/01/31. https://doi.org/10.1128/IAI.01862-06 PMID: 17261600; PubMed Central PMCID: PMC1865672.

37. Buchholz KR, Bowyer PW, Boothroyd JC. Bradyzoite pseudokinase 1 is crucial for efficient oral infectivity of the Toxoplasma gondii tissue cyst. Eukaryot Cell. 2013; 12(3):399–410. Epub 2013/01/08. https://doi.org/10.1128/EC.00343-12 PMID: 23291621; PubMed Central PMCID: PMC3629768.

38. Gubbels MJ, Lehmann M, Muthalagi M, Jerome ME, Brooks CF, Szatanek T, et al. Forward genetic analysis of the apicomplexan cell division cycle in Toxoplasma gondii. PLoS Pathog. 2008; 4(2):e36. Epub 2008/02/20. https://doi.org/10.1371/journal.ppat.0040036 PMID: 18282098; PubMed Central PMCID: PMC2242837.

39. Fox BA, Falla A, Rommereim LM, Tomita T, Gigley JP, Mercier C, et al. Type II Toxoplasma gondii KU80 knockout strains enable functional analysis of genes required for cyst development and latent infection. Eukaryot Cell. 2011; 10(9):1193–206. Epub 2011/05/03. https://doi.org/10.1128/EC.00297-10 PMID: 21531875; PubMed Central PMCID: PMC3187049.

40. Heaslip AT, Nishi M, Stein B, Hu K. The motility of a human parasite, Toxoplasma gondii, is regulated by a novel lysine methyltransferase. PLoS Pathog. 2011; 7(9):e1002201. Epub 2011/09/13. https://doi.org/10.1371/journal.ppat.1002201 PMID: 21909263; PubMed Central PMCID: PMC3164638.

41. Tomita T, Bzik DJ, Ma YF, Fox BA, Markillie LM, Taylor RC, et al. The Toxoplasma gondii cyst wall protein CST1 is critical for cyst wall integrity and promotes bradyzoite persistence. PLoS Pathog. 2013; 9 (12):e1003823. Epub 2014/01/05. https://doi.org/10.1371/journal.ppat.1003823 PMID: 24385904; PubMed Central PMCID: PMC3873430.

42. Khan A, Behnke MS, Dunay IR, White MW, Sibley LD. Phenotypic and gene expression changes among clonal type I strains of Toxoplasma gondii. Eukaryot Cell. 2009; 8(12):1828–36. https://doi.org/10.1128/EC.00150-09 PMID: 19801420; PubMed Central PMCID: PMCPMC2794221.

43. Herm-Gotz A, Agop-Nersesian C, Munter S, Grimley JS, Wandless TJ, Frischknecht F, et al. Rapid control of protein level in the apicomplexan Toxoplasma gondii. Nat Methods. 2007; 4(12):1003–5. Epub 2007/11/13. doi: nmeth1134 [pii] https://doi.org/10.1038/nmeth1134 PMID: 17994029; PubMed Central PMCID: PMC2601725.

44. Brancucci NM, Bertschi NL, Zhu L, Niederwieser I, Chin WH, Wampfler R, et al. Heterochromatin protein 1 secures survival and transmission of malaria parasites. Cell Host Microbe. 2014; 16(2):165–76. https://doi.org/10.1016/j.chom.2014.07.004 PMID: 25121746.

45. Dunay IR, Fuchs A, Sibley LD. Inflammatory monocytes but not neutrophils are necessary to control infection with Toxoplasma gondii in mice. Infect Immun. 2010; 78(4):1564–70. https://doi.org/10.1128/IAI.00472-09 PMID: 20145099; PubMed Central PMCID: PMC2849397.

46. Dunay IR, Damatta RA, Fux B, Presti R, Greco S, Colonna M, et al. Gr1(+) inflammatory monocytes are required for mucosal resistance to the pathogen Toxoplasma gondii. Immunity. 2008; 29(2):306–17. https://doi.org/10.1016/j.immuni.2008.05.019 PMID: 18691912; PubMed Central PMCID: PMCPMC2605393.

47. Dubey JP. Tissue cyst tropism in Toxoplasma gondii: a comparison of tissue cyst formation in organs of cats, and rodents fed oocysts. Parasitology. 1997; 115 (Pt 1):15–20. PMID: 9226953.

48. Speer CA, Dubey JP. Ultrastructure of early stages of infections in mice fed Toxoplasma gondii oocysts. Parasitology. 1998; 116 (Pt 1):35–42. PMID: 9481772.

49. Konradt C, Ueno N, Christian DA, Delong JH, Pritchard GH, Herz J, et al. Endothelial cells are a replicative niche for entry of Toxoplasma gondii to the central nervous system. Nature microbiology. 2016; 1:16001. https://doi.org/10.1038/nmicrobiol.2016.1 PMID: 27572166.

50. Cabral CM, Tuladhar S, Dietrich HK, Nguyen E, MacDonald WR, Trivedi T, et al. Neurons are the Primary Target Cell for the Brain-Tropic Intracellular Parasite Toxoplasma gondii. PLoS pathogens. 2016; 12(2):e1005447. https://doi.org/10.1371/journal.ppat.1005447 PMID: 26895155; PubMed Central PMCID: PMC4760770.

51. Ferguson DJ, Hutchison WM, Pettersen E. Tissue cyst rupture in mice chronically infected with Toxoplasma gondii. An immunocytochemical and ultrastructural study. Parasitol Res. 1989; 75(8):599–603. PMID: 2771928.

52. Bohne W, Heesemann J, Gross U. Reduced replication of Toxoplasma gondii is necessary for induction of bradyzoite-specific antigens: a possible role for nitric oxide in triggering stage conversion. Infect Immun. 1994; 62(5):1761–7. Epub 1994/05/01. PMID: 8168938; PubMed Central PMCID: PMC186404.

53. Biswas A, Bruder D, Wolf SA, Jeron A, Mack M, Heimesaat MM, et al. Ly6C(high) monocytes control cerebral toxoplasmosis. J Immunol. 2015; 194(7):3223–35. https://doi.org/10.4049/jimmunol.1402037 PMID: 25710908.

54. Bohne W, Holpert M, Gross U. Stage differentiation of the protozoan parasite Toxoplasma gondii. Immunobiology. 1999; 201(2):248–54. Epub 2000/01/13. https://doi.org/10.1016/S0171-2985(99)80065-5 PMID: 10631574.

55. Gross U, Bohne W, Soete M, Dubremetz JF. Developmental differentiation between tachyzoites and bradyzoites of Toxoplasma gondii. Parasitol Today. 1996; 12(1):30–3. Epub 1996/01/01. PMID: 15275305.

56. Tenter AM, Heckeroth AR, Weiss LM. Toxoplasma gondii: from animals to humans. International journal for parasitology. 2000; 30(12–13):1217–58. Epub 2000/12/13. PMID: 11113252; PubMed Central PMCID: PMC3109627.

57. Dubey JP, Murrell KD, Fayer R. Persistence of encysted Toxoplasma gondii in tissues of pigs fed oocysts. American journal of veterinary research. 1984; 45(10):1941–3. PMID: 6497091.

58. Fayer R, Frenkel JK. Comparative infectivity for calves of oocysts of feline coccidia: Besnoitia, Hammondia, Cystoisospora, Sarcocystis, and Toxoplasma. The Journal of parasitology. 1979; 65(5):756–62. PMID: 117090.

59. Behnke MS, Khan A, Wootton JC, Dubey JP, Tang K, Sibley LD. Virulence differences in Toxoplasma mediated by amplification of a family of polymorphic pseudokinases. Proc Natl Acad Sci U S A. 2011; 108(23):9631–6. Epub 2011/05/19. https://doi.org/10.1073/pnas.1015338108 PMID: 21586633; PubMed Central PMCID: PMC3111276.

60. Suvorova ES, Lehmann MM, Kratzer S, White MW. Nuclear actin-related protein is required for chromosome segregation in Toxoplasma gondii. Mol Biochem Parasitol. 2012; 181(1):7–16. Epub 2011/10/04. https://doi.org/10.1016/j.molbiopara.2011.09.006 PMID: 21963440; PubMed Central PMCID: PMC3767130.

61. Olguin-Lamas A, Madec E, Hovasse A, Werkmeister E, Callebaut I, Slomianny C, et al. A novel Toxoplasma gondii nuclear factor TgNF3 is a dynamic chromatin-associated component, modulator of nucleolar architecture and parasite virulence. PLoS Pathog. 2011; 7(3):e1001328. Epub 2011/04/13. https://doi.org/10.1371/journal.ppat.1001328 PMID: 21483487; PubMed Central PMCID: PMC3068996.

62. Lavine MD, Knoll LJ, Rooney PJ, Arrizabalaga G. A Toxoplasma gondii mutant defective in responding to calcium fluxes shows reduced in vivo pathogenicity. Mol Biochem Parasitol. 2007; 155(2):113–22. https://doi.org/10.1016/j.molbiopara.2007.06.004 PMID: 17643508; PubMed Central PMCID: PMCPMC2034501.

63. Wilson EH, Wille-Reece U, Dzierszinski F, Hunter CA. A critical role for IL-10 in limiting inflammation during toxoplasmic encephalitis. J Neuroimmunol. 2005; 165(1–2):63–74. https://doi.org/10.1016/j.jneuroim.2005.04.018 PMID: 16005735.

64. Behnke MS, Radke JB, Smith AT, Sullivan WJ Jr., White MW. The transcription of bradyzoite genes in Toxoplasma gondii is controlled by autonomous promoter elements. Mol Microbiol. 2008; 68(6):1502–18. https://doi.org/10.1111/j.1365-2958.2008.06249.x PMID: 18433450.